

Journal of Computational Acoustics  
 © IMACS

## A TIME DOMAIN METHOD FOR MODELING VISCOACOUSTIC WAVE PROPAGATION

Jean-Philippe GROBY

*Laboratoire de Mécanique et d'Acoustique,  
 31 Chemin Joseph Aiguier, 13402 Marseille Cedex 20, FRANCE  
 groby@lma.cnrs-mrs.fr*

Chrysoula TSOGKA

*Mathematics Department, Stanford University,  
 Stanford, CA 94305, USA  
 tsogka@math.Stanford.EDU*

In many applications, and in particular in seismology, realistic propagation media disperse and attenuate waves. This dissipative behavior can be taken into account by using a viscoacoustic propagation model, which incorporates a complex and frequency-dependent viscoacoustic modulus in the constitutive relation. The main difficulty then lies in finding an efficient way to discretize the constitutive equation as it becomes a convolution integral in the time domain. To overcome this difficulty the usual approach consists in approximating the viscoacoustic modulus by a low-order rational function of frequency. We use here such an approximation and show how it can be incorporated in the velocity-pressure formulation for viscoacoustic waves. This formulation is coupled with the fictitious domain method which permit us to model efficiently diffraction by objects of complicated geometry and with the Perfectly Matched Layer Model which allows us to model wave propagation in unbounded domains. The space discretisation of the problem is based on a mixed finite element method and for the discretisation in time a 2nd order centered finite difference scheme is employed. Several numerical examples illustrate the efficiency of the method.

*Keywords:* viscoacoustic; time domain method.

### 1. Introduction

Real media attenuate and disperse propagating waves<sup>1</sup>. Our aim in this paper is to develop a numerical method to model such dissipative phenomena (dispersion plus attenuation) in the time domain. To do so we consider the linear viscoacoustic equation which is a convolution in the time domain, the viscoacoustic modulus being frequency dependent. Therefore, incorporating any arbitrary dissipation law in time-domain methods is in general computationally intense. The usual way to overcome this difficulty is to approximate the viscoacoustic modulus by a low-order rational function<sup>2,3,4,5</sup>. This leads to replacing the convolution integral by a set of variables, usually referred to as memory variables, which satisfy simple differential equations that can be easily discretized in the time domain.

Several methods have been proposed in the literature for incorporating realistic attenuation laws (e.g. frequency-independent or weakly frequency-dependent viscoacoustic modulus) into time-domain methods<sup>2,3,5,4,6,7</sup>. We focus our attention in this paper on the methods

proposed by Day and Minster (1984), Emmerich and Korn (1987), and Blanch, Robertson and Symes (1995). All three methods use some approximation of the viscoacoustic modulus by a low-order rational function. The first approach is based on the standard Padé approximation. The coefficients of the rational approximation are thus in principle known analytically. Numerical results obtained using this method show that the approximation is poor and the method provides satisfactory results only for relatively short (in terms of the wavelength) propagation paths. The second approach is based on the rheological model of the generalized Maxwell body, which gives a physical meaning to the coefficients of the rational approximation. They are interpreted as the relaxation frequencies and weight factors of the classical Maxwell bodies, which form the generalized Maxwell body. This method provides good numerical results for long propagation paths, but some parameters, namely the relaxation frequencies are semi-empirically determined. Finally, the third method is based on the observation that for the frequency-independent case and for weakly attenuating materials the weight factors are only slowly varying and can be approximated by a constant. This method provides good numerical results, but also involves a semi-empirical choice of a parameter.

Although, the previous methods give satisfactory results in the case of weakly-attenuating materials they fail in media with large attenuation. This case was considered in a recent paper <sup>8</sup>, where the authors propose an analytic method for computing the best (optimal) rational approximation for the frequency independent case. They also propose a generalization of the algorithm presented in <sup>3</sup> which leads to very good results in the case of highly attenuating media and a frequency- dependent viscoacoustic modulus.

After a brief overview of the basic theory describing wave propagation in viscoacoustic media (section 2), we describe in section 3 the approximations proposed in <sup>2</sup>, <sup>3</sup> and <sup>5</sup>.

Considering long propagation paths, we test the performance of the different approximations and find that the best method, using the smaller number of unknowns while providing satisfactory numerical results and involving the least number of empirically determined values, is the one proposed by Emmerich and Korn (1987). We thus chose this method for approximating the viscoacoustic modulus. Note that a slight variation of the method proposed in <sup>3</sup> is used here, based on a different way of distributing the relaxation frequencies in the bandwidth of the incident pulse.

In section 4 we incorporate this approximation in the velocity-pressure formulation for viscoacoustic waves. Our choice of using the first-order-in-time system of equations, instead of the more classical second-order one, is motivated by the use of the fictitious domain method and the perfectly matched absorbing layer technique. In <sup>9</sup> the authors proposed a similar approach using the mixed velocity-stress formulation for modeling wave propagation in viscoelastic media.

The term fictitious domain method (also called domain embedding method) was initially introduced by V.K. Saul'ev in <sup>10</sup>, where the solution of an elliptic problem in a domain with complex geometry was considered. The general idea of this method consists in replacing the original problem by an equivalent one for which the solution is sought in an enlarged domain (i.e., containing the initial one) with a simple geometry. The idea to use Lagrange

multipliers in the framework of the fictitious domain method was first introduced in <sup>11</sup>. Since then the method has been used in several frameworks for solving problems involving complex geometries <sup>12,13,14,15</sup>, and, in particular, for wave propagation problems <sup>16,17,18,19</sup>. In the framework of seismic wave propagation we apply this method to model the boundary condition on the surface of the earth (section 7). Its main feature is extending the solution to a domain with simple shape, independent of the complex geometry, and to impose the boundary conditions with the introduction of a Lagrange multiplier. Thus, the solution is determined by two types of unknowns, the extended unknowns, defined in the enlarged simple shape domain and the auxiliary variable, supported on the boundary of complex geometry. The main advantage is that the mesh for computing the extended functions can now be chosen independently of the geometry of the boundary.

The Perfectly Matched Layers (PML) technique was introduced by Bérenger <sup>20,21</sup> for Maxwell's equations and is now the most widely-used method for the simulation of electromagnetic waves in unbounded domains (cf. <sup>22,23,24</sup>). It has also been extended to the case of anisotropic acoustic waves <sup>25</sup>, isotropic <sup>26</sup> and anisotropic elastic waves <sup>27,25</sup>. This technique consists in designing an absorbing layer, called a perfectly matched layer (PML), that has the property of generating *no reflection* at the interface between the free medium and the artificial absorbing medium. This property allows the use of a very high damping parameter inside the layer, and consequently of a small layer width, while achieving a near-perfect absorption of the waves. We apply here the PML model in the case of viscoacoustic waves (section 8).

Another advantage of the first-order formulation over the second order one, is that it is easier to implement in heterogeneous media, since it does not require an approximation of spatial derivatives of the physical parameters. To discretize this formulation in space we use a mixed finite-element method which is a modification of the method proposed in <sup>28</sup>. More precisely, in <sup>28</sup> the authors designed new mixed finite elements, the so-called  $Q_{k+1}^{div} - Q^k$  elements, inspired by Nédélec's second family <sup>29</sup>, which are compatible with mass lumping, and therefore allow to construct an explicit scheme in time. A non-standard convergence analysis of the  $Q_{k+1}^{div} - Q^k$  elements was carried out in <sup>28</sup>. However, numerical results obtained recently (cf. <sup>30</sup>) show that, when coupled with the fictitious domain method, these elements do not provide satisfactory results. This is why we use here instead the  $Q_{k+1}^{div} - P^{k+1}$  elements for which convergence of the fictitious domain method was obtained <sup>30</sup>.

To show the efficiency and robustness of the method we present in section 9 several numerical results. In particular, numerical and analytical results are compared and good agreement is obtained between the two.

## 2. Viscoacoustic wave propagation

In an isotropic viscoacoustic medium occupying a domain  $\Omega \in \mathbb{R}^d$ ,  $d = 1, 2, 3$ , the relation between the pressure  $p(\omega) = p(\mathbf{x}, \omega)$  and the displacement  $\mathbf{u}(\omega) = \mathbf{u}(\mathbf{x}, \omega)$  in the frequency domain is,

$$p(\omega) = \mu(\mathbf{x}, \omega) \operatorname{div} \mathbf{u}(\omega). \quad (1)$$

Here,  $\mu(\mathbf{x}, \omega)$  is the complex, frequency-dependent, viscoacoustic modulus.

The dissipative aspect of a material is often described by the quality factor  $Q$ , defined as the ratio of the real and imaginary parts of the viscoacoustic modulus. It expresses how attenuating a material is and corresponds to the number of wavelengths a wave can propagate through the medium before its amplitude has decreased by  $e^{-\pi}$ ,

$$Q(\mathbf{x}, \omega) = \frac{\Re(\mu(\mathbf{x}, \omega))}{\Im(\mu(\mathbf{x}, \omega))} = \frac{1}{\tan(\phi(\mathbf{x}, \omega))}, \quad (2)$$

where  $\phi(\mathbf{x}, \omega)$  is the phase of  $\mu(\mathbf{x}, \omega)$ .

In seismic applications,  $Q$  is usually assumed to be frequency-independent or only slowly frequency-dependent. In this case (i.e. when  $Q$  is constant in frequency), the viscoacoustic modulus is given analytically by Kjartansson's model<sup>31</sup>,

$$\mu(\mathbf{x}, \omega) = \mu_{ref} \left( \frac{\mathbf{i}\omega}{\omega_{ref}} \right)^{\frac{2}{\pi} \arctan(Q^{-1})}. \quad (3)$$

This analytical formulation will be useful for validation of the numerical results in the next sections.

In the time domain, the constitutive relation (1) is expressed in terms of a convolution operator, denoted here by  $\star_t$ ,

$$p(\mathbf{x}, t) = \mu(\mathbf{x}, t) \star_t \operatorname{div} \mathbf{u}(\mathbf{x}, t). \quad (4)$$

The discretisation of this equation requires saving in memory the whole history of the solution at all points of the computational domain and is thus very expensive. To overcome this inconvenience, we approximate the viscoacoustic modulus by a rational function in frequency, as was proposed in<sup>2,3,4,5</sup>. It is convenient in the following to introduce the relaxation function  $R(\mathbf{x}, t)$ , defined by, (see Figure 1),

$$\mu(\mathbf{x}, t) = \frac{\partial R(\mathbf{x}, t)}{\partial t}; \quad R(\mathbf{x}, t) = \left( \mu_R(\mathbf{x}) + \delta\mu(\mathbf{x}) \int_0^{+\infty} r(\mathbf{x}, \omega') e^{-\omega' t} d\omega' \right) H(t), \quad (5)$$

where  $\mu_R$  is the relaxed modulus,

$$\mu_R(\mathbf{x}) = \lim_{t \rightarrow +\infty} R(\mathbf{x}, t),$$

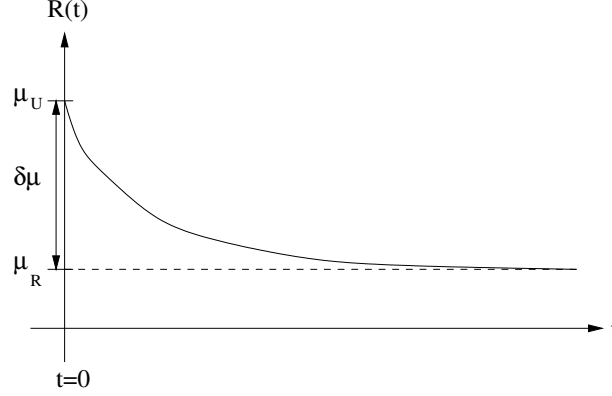
$\mu_U$  is the unrelaxed modulus,

$$\mu_U(\mathbf{x}) = \mu_R(\mathbf{x}) + \delta\mu(\mathbf{x}) = \lim_{t \rightarrow 0} R(\mathbf{x}, t),$$

$r(\mathbf{x}, \omega')$  is the normalized relaxation spectrum satisfying

$$\int_0^{+\infty} r(\mathbf{x}, \omega') d\omega' = 1,$$

and  $H(t)$  is the Heaviside function.


 Fig. 1. Schematic example of the relaxation function  $R(t)$ 

Using  $\mu(\mathbf{x}, t)$  defined by (5) in (4) gives,

$$p(\mathbf{x}, t) = \mu_U(\mathbf{x}) \operatorname{div} \mathbf{u}(\mathbf{x}, t) - \delta\mu(\mathbf{x}) \int_{-\infty}^t \int_0^{+\infty} \omega' r(\mathbf{x}, \omega') e^{-\omega'(t-\tau)} \operatorname{div} \mathbf{u}(\mathbf{x}, \tau) d\omega' d\tau.$$

We now assume that the relaxation spectrum can be discretised by  $L$  single peaks of amplitude  $\alpha_l$  at relaxation frequencies  $\omega_l$ ,  $l \in [1 \dots L]$ ,

$$r(\mathbf{x}, \omega) = \sum_{l=1}^L \alpha_l(\mathbf{x}) \delta(\omega - \omega_l(\mathbf{x})) ; \sum_{l=1}^L \alpha_l(\mathbf{x}) = 1,$$

In this case, we get,

$$R(\mathbf{x}, t) \simeq R_l(\mathbf{x}, t) = \left( \mu_R(\mathbf{x}) + \delta\mu(\mathbf{x}) \sum_{l=1}^L \alpha_l(\mathbf{x}) e^{-\omega_l(\mathbf{x})t} \right) H(t),$$

and

$$\mu(\mathbf{x}, \omega) \simeq \mu_l(\mathbf{x}, \omega) = \mu_R(\mathbf{x}) \left( 1 + \sum_{l=1}^L \frac{y_l(\mathbf{x}) \mathbf{i}\omega}{\mathbf{i}\omega + \omega_l(\mathbf{x})} \right). \quad (6)$$

In (6), we introduced  $y_l(\mathbf{x})$  defined by,

$$y_l(\mathbf{x}) = \frac{\delta\mu(\mathbf{x})}{\mu_R(\mathbf{x})} \alpha_l(\mathbf{x}), \text{ with the normalization relation } \sum_{l=1}^L y_l(\mathbf{x}) = \frac{\delta\mu(\mathbf{x})}{\mu_R(\mathbf{x})}.$$

Notice that equation (6) can be obtained if one assumes that  $\mu(\mathbf{x}, \omega)$  can be approximated by a rational function of  $(\mathbf{i}\omega)$ ,

$$\mu(\mathbf{x}, \omega) \simeq \mu_l(\mathbf{x}, \omega) = \frac{P_L(\mathbf{x}, \mathbf{i}\omega)}{Q_L(\mathbf{x}, \mathbf{i}\omega)}, \quad (7)$$

with  $P_L$  and  $Q_L$  being polynomials of degree  $L$  in  $(i\omega)$ . Then (6) can be interpreted as an expansion of (7) into partial fractions<sup>3</sup>. Thus approximating the viscoacoustic modulus by a rational function is equivalent to approximating the relaxation spectrum by a discrete one.

For computational reasons, it is natural to search for rational function approximations of the viscoacoustic modulus, which minimize the ratio: number of unknowns/accuracy. We therefore address in the following the question of finding an accurate low-order approximation of the viscoacoustic modulus.

### 3. Approximation of the viscoacoustic modulus

We now briefly introduce the different approximation methods previously proposed in the literature.

#### 3.1. Padé approximation method

The use of the simple Padé approximation in the framework of viscoacoustic wave propagation was proposed in<sup>2</sup>. Letting  $z = -\frac{1}{i\omega}$  and introducing,

$$\chi(\mathbf{x}, z) = \int_0^{+\infty} \frac{\omega' r(\mathbf{x}, \omega')}{1 - \omega' z} d\omega',$$

$\mu(\mathbf{x}, \omega)$  can be re-written in the following form,

$$\mu(\mathbf{x}, \omega) = \mu_U(\mathbf{x}) + \delta\mu(\mathbf{x})z\chi(\mathbf{x}, z).$$

The Padé approximation is then used for expanding  $\chi(\mathbf{x}, z)$  into a rational function with numerator of degree  $L - 1$  and denominator of degree  $L$ . Using the well-known<sup>(32,33)</sup> relations between Padé approximations and orthogonal polynomials one gets,

$$\chi(\mathbf{x}, z) = \sum_{l=1}^L \frac{\lambda_l(\mathbf{x})}{1 - \omega_l(\mathbf{x})z},$$

where  $\omega_l$  are the zeros of the orthogonal polynomial  $P_L$ , and  $\lambda_l$  are the residuals given by,

$$\lambda_l(\mathbf{x}) = \frac{k_L}{k_{L-1}P_{L-1}(\omega_l(\mathbf{x}))P_L'(\omega_l(\mathbf{x}))},$$

$k_L$  being the leading coefficient of  $P_L$  and where the prime denotes the derivative of  $P_L$ . Recall that the orthogonal polynomials are defined by,

$$\int_{\Omega_1}^{\Omega_2} P_n(\omega')P_m(\omega')\omega' r(\omega')d\omega' = \delta_{mn},$$

where  $\delta_{mn}$  is the Kronecker symbol. When the quality factor is constant over a frequency band,  $\lambda_l$  and  $\omega_l$  can be obtained in closed form. Moreover, when  $Q \ll 1$ , the relaxation

spectrum  $r(\mathbf{x}, \omega)$  is proportional to  $\omega^{-1}$ . Assuming that  $r(\mathbf{x}, \omega)$  is zero outside the frequency interval  $[\Omega_1, \Omega_2]$  we obtain the approximation,

$$\mu(\mathbf{x}, \omega) \simeq \mu_l(\omega) = \mu_U \left( 1 - \frac{\Omega_2 - \Omega_1}{\pi Q} \sum_{l=1}^L \frac{\nu_l(\mathbf{x})}{i\omega + \omega_l(\mathbf{x})} \right), \quad (8)$$

where  $\omega_l = \frac{1}{2}[x_l(\Omega_2 - \Omega_1) + \Omega_2 + \Omega_1]$ ,  $x_l$  and  $\nu_l$  being respectively the zeros and weights of the Legendre polynomials. Notice that the relaxation frequencies  $\omega_l$  are in this case equidistant on a linear scale. The main advantage of this approximation is that all data are analytically determined. For more details on this method the reader can refer to <sup>2</sup>.

### 3.2. Generalized Maxwell Body approximation method

We describe here the method proposed in <sup>3</sup>. First let us re-write (6) as,

$$\mu_l(\mathbf{x}, \omega) = \mu_R(\mathbf{x}) + \delta\mu(\mathbf{x}) \sum_{l=1}^L \frac{\alpha_l(\mathbf{x})\mathbf{i}\omega}{\mathbf{i}\omega + \omega_l(\mathbf{x})}. \quad (9)$$

Each term of (9) can be interpreted as a classical Maxwell body with viscosity  $\alpha_l \frac{\delta\mu}{\omega_l}$  and elastic modulus  $\alpha_l \delta\mu$ . The term  $\mu_R$  in (9) represents an additional elastic element. The  $Q$ -law for the generalized Maxwell body approximation can be obtained from (9),

$$Q(\mathbf{x}, \omega)^{-1} = \frac{\Im(\mu(\mathbf{x}, \omega))}{\Re(\mu(\mathbf{x}, \omega))} = \frac{\sum_{l=1}^L y_l(\mathbf{x}) \frac{\frac{\omega}{\omega_l(\mathbf{x})}}{1 + (\frac{\omega}{\omega_l(\mathbf{x})})^2}}{1 + \sum_{l=1}^L y_l(\mathbf{x}) \frac{(\frac{\omega}{\omega_l(\mathbf{x})})^2}{1 + (\frac{\omega}{\omega_l(\mathbf{x})})^2}}. \quad (10)$$

Assuming now that  $\delta\mu \ll \mu_R$ , (10) becomes,

$$Q(\mathbf{x}, \omega)^{-1} \simeq \frac{\delta\mu(\mathbf{x})}{\mu_R(\mathbf{x})} \sum_{l=1}^L \alpha_l(\mathbf{x}) \frac{\frac{\omega}{\omega_l(\mathbf{x})}}{1 + (\frac{\omega}{\omega_l(\mathbf{x})})^2}. \quad (11)$$

This means that  $Q(\omega)^{-1}$  is approximately the sum of  $L$  Debye functions with maxima  $\alpha_l \frac{\delta\mu}{2\mu_R}$  located at frequencies  $\omega_l$ . If  $Q$  is fairly constant in a frequency band, the most natural choice for the relaxation frequencies  $\omega_l$  is a logarithmic equidistant distribution. In this case, to obtain a good approximation of  $Q(\omega)^{-1}$ , the distance between two adjacent relaxation frequencies should be chosen smaller or equal to the half-width of the Debye function (1.144 decades). In <sup>3</sup> two ways for choosing  $\omega_l$  were proposed:  $\omega_l$  can be chosen logarithmically-equidistant in the frequency band  $[\Omega_1, \Omega_2]$  or determined by  $\omega_l = \frac{2\omega_{dom}}{10^l}$  where  $\omega_{dom}$  is the dominant (central) frequency of the source considered in the simulations. In both cases, the coefficients  $y_l$  are obtained by solving the overdetermined linear system

$$\sum_{l=1}^L y_l(\mathbf{x}) \tilde{\omega}_k(\mathbf{x}) \frac{\omega_l(\mathbf{x}) - \tilde{Q}^{-1}(\mathbf{x}, \tilde{\omega}_k(\mathbf{x})) \tilde{\omega}_k(\mathbf{x})}{\omega_l(\mathbf{x})^2 + \tilde{\omega}_k(\mathbf{x})^2} = \tilde{Q}^{-1}(\mathbf{x}, \tilde{\omega}_k(\mathbf{x})), \quad k \in [1, 2, \dots, K = 2L - 1], \quad (12)$$

8 *J.-P. GROBY and C. TSOGKA*

where,  $\tilde{\omega}_k$  are defined by

$$\begin{aligned}\tilde{\omega}_1 &= \Omega_1, \\ \tilde{\omega}_{k+1} &= \tilde{\omega}_k \left( \frac{\Omega_2}{\Omega_1} \right)^{\frac{1}{2}}.\end{aligned}$$

Let us remark that the determination of  $\omega_l$  for this approximation is based on an empirical study.

### 3.3. The $\tau$ -method

This method, proposed in <sup>5</sup> is based on the observation that dissipation due to only one “Maxwell Body” can be determined by a unique dimensionless parameter  $\tau$ . More precisely, for  $Q \gg 1$  and  $L = 1$ , equation (11) becomes,

$$Q(\mathbf{x}, \omega)^{-1} = \frac{\frac{\omega}{\omega_1(\mathbf{x})} \tau(\mathbf{x})}{1 + \left( \frac{\omega}{\omega_1(\mathbf{x})} \right)^2},$$

where  $\tau = y_1 \ll 1$ . It is then easy to see (cf. <sup>5</sup>), that  $\omega_1$  essentially determines the frequency behavior of  $Q$  while  $\tau$  determines its magnitude. In the general case for  $L > 1$ , and when one seeks an approximation of a constant  $Q$  value,  $y_l$  are quasi-constant and equation (11) can be approximated by,

$$Q(\mathbf{x}, \omega)^{-1} = \sum_{l=1}^L \frac{\frac{\omega}{\omega_l(\mathbf{x})} \tau(\mathbf{x})}{1 + \left( \frac{\omega}{\omega_l(\mathbf{x})} \right)^2}. \quad (13)$$

In (13),  $Q(\omega)^{-1}$  is linear in  $\tau$ . One can therefore find the best approximation, in the least-squares sense, over a predefined frequency range to any  $Q_0$  by minimizing over  $\tau$  the expression,

$$J = \int_{\Omega_1}^{\Omega_2} (Q^{-1}(\omega, \omega_l, \tau) - Q_0^{-1})^2 d\omega. \quad (14)$$

The approximation of the viscoacoustic modulus in this case is,

$$\mu_l(\mathbf{x}, \omega) = \mu_R(\mathbf{x}) \left( 1 + \sum_{l=1}^L \frac{\tau(\mathbf{x}) \mathbf{i}\omega}{\mathbf{i}\omega + \omega_l(\mathbf{x})} \right). \quad (15)$$

The relaxation frequencies  $\omega_l$  are chosen, as for the “Generalized Maxwell Body” method, equidistant on a logarithmic scale. Equation (15) leads in general to an over-estimation of the value of  $Q$ . Thus the authors in <sup>5</sup> suggest to use in the definition of  $J$  (14) a value for  $Q_0$  slightly smaller than the desired one. This value is also chosen empirically.

### 3.4. Comparison of the different approximation methods

To test the accuracy of the different approximation methods previously presented, we compute the response of a one-dimensional viscoacoustic homogeneous medium to the following pulse,

$$s(t) = \sin\left(\frac{2\pi t}{T}\right) - 0.5\sin\left(\frac{4\pi t}{T}\right) \text{ for } 0 < t < T, T = 0.3s. \quad (16)$$

The solution is obtained by convolving the source function  $s(t)$  with the dissipation operator  $D(t)$  (the Green's function for the 1D problem). For an arbitrary dissipation law, the Fourier transform  $D(\omega)$  of  $D(t)$  is given by <sup>3</sup>,

$$D(\omega) = e^{i\omega t^* Q(\omega_r) \left(1 - \frac{c(\omega_r)}{\nu(\omega)}\right)}, \quad (17)$$

where  $c(\omega_r)$  is the phase velocity at the reference frequency  $\omega_r$ ,  $\nu(\omega)$  the complex velocity, and  $t^* = \frac{x}{c(\omega_r)Q(\omega_r)}$  the dissipation time. For a frequency independent  $Q$ , the value of  $\frac{c(\omega_r)}{\nu(\omega)} = \left(\frac{|\mu(\omega_r)|}{\mu(\omega)}\right)^{1/2}$ , can be determined from equation (3) combined with one of (8), (15) or (6)-(12) depending on the approximation method used. We recall that all methods have as common starting point relation (6) from where the Padé approximation leads to (8) and the  $\tau$ -method to (15). The Maxwell body approximation is given by (6) with the coefficients  $y_l$  computed from (12).

In the numerical example, we want to approximate  $Q = 20$  over the frequency range  $[10^{-2}, 10^2]$  Hz, like in <sup>3</sup>. To better illustrate the results, we present in Figure 2 the evolution of the correlation coefficient between the exact solution (the one obtained for the viscosity modulus calculated from (3)) and the different approximated ones as a function of the dissipation time.

More precisely in Figure 2 we compare the results obtained with the following approximations,

- Padé approximation with  $L = 5$ .
- Method 1: Maxwell Body approximation with  $L = 3$ . Although we want to approximate  $Q = 20$  over the frequency range  $[10^{-2}, 10^2]$  Hz, we follow here the method proposed in <sup>3</sup> and choose the relaxation frequencies logarithmically-equidistant over the frequency range  $[10^{-1.5}, 10^{1.5}]$  Hz. The key point is that ideally  $\omega_j$  should be placed at distance smaller or equal to half width of the Debey functions (1.144 decades) which is not possible with  $L = 3$  in the interval  $[10^{-2}, 10^2]$ . Although this criterion is not satisfied with  $L = 3$  in  $[10^{-1.5}, 10^{1.5}]$  either, the approximation obtained is fairly good.
- Method 2: Maxwell Body approximation with  $L = 3$  and relaxation frequencies chosen equidistant on a logarithmic scale, such that,  $\omega_l = \frac{2\omega_{dom}}{10^l}$ . This method was also proposed in <sup>3</sup> and gives slightly better results than method 1. Note that in this case the criterion on the maximum distance between  $\omega_j$  is respected.

- The  $\tau$ -method with  $Q_0 = 17.6$  (value proposed in <sup>5</sup> to model the propagation in a viscoacoustic medium with  $Q = 20$ ) and  $L = 3$ .

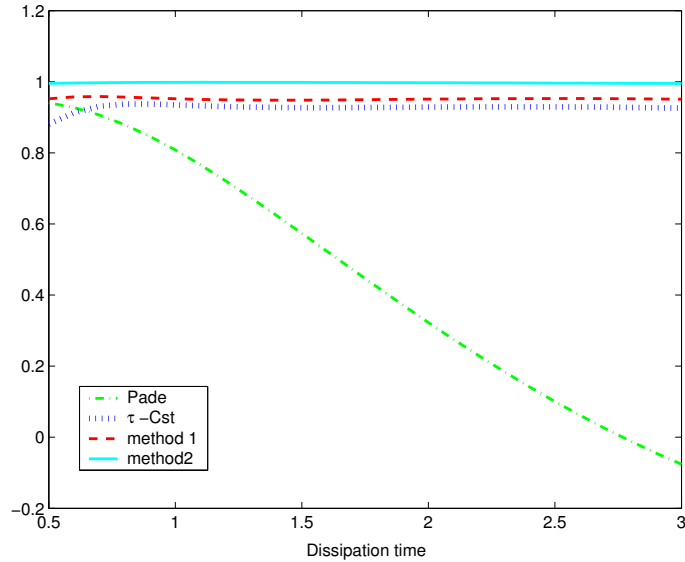


Fig. 2. Comparison between the different approximation methods. Correlation coefficient between the exact and the approximated solutions as a function of the dissipation time.

The results illustrated in Figure 2, show that the Padé approximant provides good accuracy only for short dissipation times, as demonstrated in <sup>3</sup>. The  $\tau$ -method provides a good accuracy/number of calculations ratio. However, we did not choose this method because  $Q_0$  has to be calibrated empirically in order to get good results. The “Generalized Maxwell Body” approximation method seems to be a good compromise between accuracy, number of calculations, and implementation simplicity. As our aim is to simulate viscoacoustic wave propagation in heterogeneous media for large dissipation times, we chose a method which is a hybrid of the Maxwell approximation methods 1 and 2.

### 3.5. Proposed method

In practice, the source type used depends on the application of interest. In our case, the main application of interest is seismic wave propagation for which a Ricker wavelet (or a time derivative of Ricker wavelet) is often used as source function,

$$f(t) = -2\alpha^2 \left( 1 - 2\alpha^2 \left( t - \frac{1}{f_0} \right)^2 \right) \exp \left( -\alpha^2 \left( t - \frac{1}{f_0} \right)^2 \right), \text{ for } 0 < t \leq \frac{2}{f_0}, \text{ with } \alpha = \pi f_0. \quad (18)$$

In Figures 3 and 4 we display the source function (18) and its spectrum for two different values of  $f_0$ . Compared to the source function defined by (16), the Ricker wavelet has a

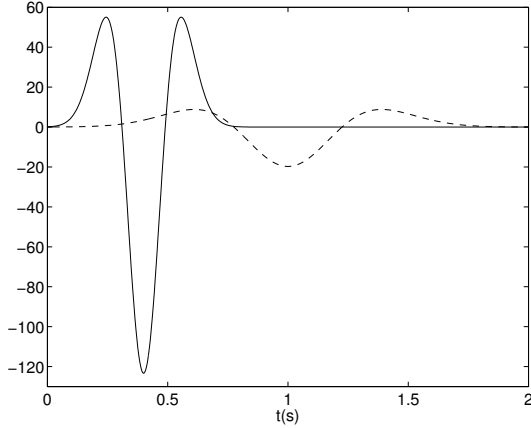


Fig. 3. The Ricker wavelet  $f(t)$  for  $f_0 = 2.5\text{Hz}$  (solid line) and for  $f_0 = 1\text{Hz}$  (dashed line).

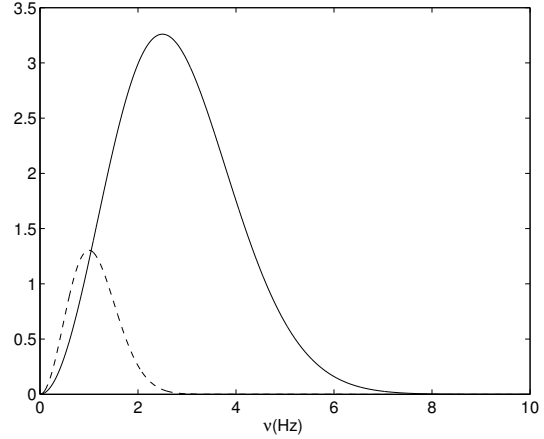


Fig. 4. The frequency spectrum of the Ricker wavelet for  $f_0 = 2.5\text{Hz}$  (solid line) and for  $f_0 = 1\text{Hz}$  (dashed line).

broader frequency spectrum and method 2 did not give as good results in this case as the ones obtained with the source (16). Following the ideas in <sup>3</sup>, we want to find a way to choose the frequency band  $[\Omega_1, \Omega_2]$  as a function of the source type and then determine the relaxation frequencies  $\omega_l$  logarithmically equidistant in this bandwidth. We found that a good choice for a Ricker wavelet type of source is  $[\Omega_1, \Omega_2] = [\frac{\omega_{max}}{100}, \omega_{max}]$ , where  $\omega_{max}$  is the maximal frequency of the employed source spectrum. To illustrate the improvement in the results, we compare in Figure 5 the proposed method with method 2 for a Ricker wavelet with  $f_0 = 2.5\text{Hz}$ .

None of the above approximation methods is completely satisfactory in our opinion because the choice of the relaxation frequencies is always empirical. To avoid this, one can follow the approach proposed in <sup>8</sup> where a non-linear minimization problem is considered which permits to determine all the coefficients (both  $y_l$  and  $\omega_l \forall l \in [1, L]$ ). However, this method is more expensive and although it improves the accuracy of the solution for media with high damping ( $Q \leq 10$ ) it provides quite similar results with the proposed method for propagation in weakly attenuating media ( $Q \geq 10$ ) <sup>8</sup>. As we are interested in media with quality factors greater than 10, we will use in the following the linear minimization method (system (12)).

#### 4. The mixed velocity-pressure formulation

By incorporating (6) into (1) we get,

$$p(\mathbf{x}, \omega) = \mu_R(\mathbf{x}) \operatorname{div}(\mathbf{u}(\mathbf{x}, \omega)) + \mu_R(\mathbf{x}) \sum_{l=1}^L \frac{y_l(\mathbf{x}) \mathbf{i}\omega}{\mathbf{i}\omega + \omega_l(\mathbf{x})} \operatorname{div}(\mathbf{u}(\mathbf{x}, \omega)). \quad (19)$$

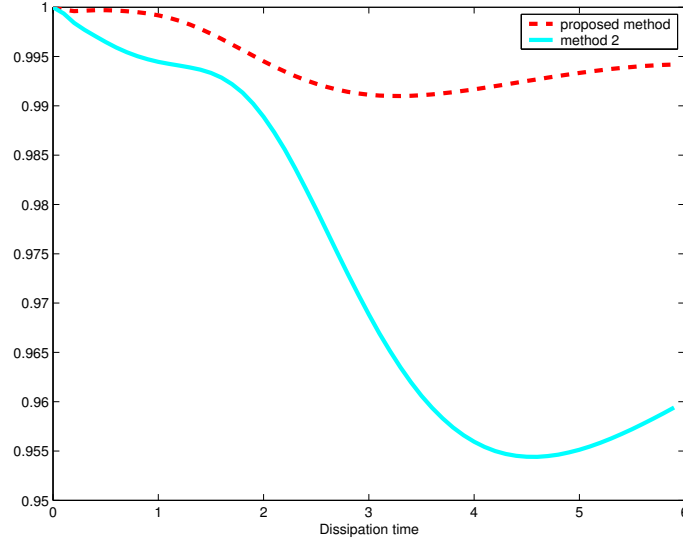


Fig. 5. Comparison between the proposed method and method 2. We display the correlation coefficient between the exact and the approximated solutions as a function of the dissipation time. The source used is a Ricker wavelet with  $f_0 = 2.5\text{Hz}$ .

We now introduce the memory variables  $\eta_l$  defined by,

$$(\mathbf{i}\omega + \omega_l(\mathbf{x}))\eta_l(\mathbf{x}, \omega) = \mu_R(\mathbf{x})y_l(\mathbf{x})\text{div}(\mathbf{v}(\mathbf{x}, \omega)), \quad (20)$$

where  $\mathbf{v}$  is the velocity, i.e., the time derivative of the displacement  $\mathbf{u}$ . Equation (20) in the time domain becomes,

$$\frac{\partial \eta_l(\mathbf{x}, t)}{\partial t} + \omega_l(\mathbf{x})\eta_l(\mathbf{x}, t) = \mu_R(\mathbf{x})y_l(\mathbf{x})\text{div}(\mathbf{v}(\mathbf{x}, t)). \quad (21)$$

Using the definition of  $\eta_l$  and multiplying (19) by  $(\mathbf{i}\omega)$ , we get,

$$(\mathbf{i}\omega)p(\mathbf{x}, \omega) = \mu_R(\mathbf{x})\text{div}(\mathbf{v}(\mathbf{x}, \omega)) + \sum_{l=1}^L (\mathbf{i}\omega)\eta_l(\mathbf{x}, \omega),$$

or equivalently in the time domain,

$$\frac{\partial p}{\partial t} = \mu_R\text{div}(\mathbf{v}) + \sum_{l=1}^L \frac{\partial \eta_l}{\partial t}. \quad (22)$$

Combining (22), (21) and the equation of motion, we obtain our final system of equations,

$$\begin{cases} \rho \frac{\partial \mathbf{v}}{\partial t} - \nabla p = \mathbf{f} & \text{in } \Omega \times ]0, T], \\ \frac{\partial p}{\partial t} - \sum_{l=1}^L \frac{\partial \eta_l}{\partial t} = \mu_R \operatorname{div}(\mathbf{v}) & \text{in } \Omega \times ]0, T], \\ \frac{\partial \eta_l}{\partial t} + \omega_l \eta_l = \mu_R y_l \operatorname{div}(\mathbf{v}), \forall l & \text{in } \Omega \times ]0, T], \end{cases} \quad (23)$$

together with initial conditions  $v(x, t = 0) = v_0(x)$ ,  $p(x, t = 0) = p_0(x)$ ,  $\eta_l(x, t = 0) = \eta_l^0(x)$ , which are zero in the examples presented in this paper, and some boundary conditions on  $\partial\Omega$  that will be precised in section 7.

Equivalently, one can choose to eliminate the pressure and obtain a second-order-in-time equation for the displacement by introducing adequate memory variables<sup>3</sup>. We prefer, however, the first-order velocity-pressure formulation for the following reasons,

- It can be coupled with the fictitious domain method for taking into account diffraction by objects of complicated geometry.
- A perfectly matched layer model (PML) can be written for this system. This permits us to simulate efficiently wave propagation in unbounded domains.
- This system is easier to implement in heterogeneous media, since it does not require an approximation of the spatial derivatives of the physical parameters.

An equivalent first-order velocity-pressure system is proposed in<sup>4</sup> and<sup>5</sup>. In<sup>4</sup> the authors used a pseudospectral method for the discretisation while in<sup>5</sup> a staggered finite difference scheme was used. Our aim being to couple this system with the fictitious domain method, we propose here instead the use of a mixed-finite element method on regular grids. A similar approach was proposed in<sup>9</sup> where the authors use a mixed-finite element method to discretise the velocity-stress formulation for viscoelastic wave propagation.

## 5. Discretisation

A mixed formulation associated to equations (23) is given by,

$$\begin{cases} \text{Find } (\mathbf{v}, p, H) : ]0, T[ \longrightarrow X \times M \times (M)^L \text{ s.t. :} \\ \frac{d}{dt}(\rho \mathbf{v}, \mathbf{w}) + b(\mathbf{w}, p) = (\mathbf{f}, \mathbf{w}), & \forall \mathbf{w} \in X, \\ \frac{d}{dt}(\frac{1}{\mu_R} p, q) - \sum_{l=1}^L \frac{d}{dt}(\frac{1}{\mu_R} \eta_l, q) - b(\mathbf{v}, q) = 0, & \forall q \in M, \\ \frac{d}{dt}(\frac{1}{\mu_R y_l} \eta_l, q) + (\frac{\omega_l}{\mu_R y_l} \eta_l, q) - b(\mathbf{v}, q) = 0, \forall l, & \forall q \in M, \end{cases} \quad (24)$$

where  $H$  is the  $L$ -dimensional vector with components  $\eta_l$ , and

$$b(\mathbf{w}, q) = \int_{\Omega} q \operatorname{div} \mathbf{w} \, d\mathbf{x}, \forall (\mathbf{w}, q) \in X \times M.$$

The functional spaces are  $X = H(\operatorname{div}; \Omega)$ , and  $M = L^2(\Omega)$ .

We now introduce some finite element spaces  $X_h \subset X$  and  $M_h \subset M$  with basis functions  $B_{N_1} = \{w_i\}_{i=1}^{N_1}$  and  $B_{N_2} = \{q_i\}_{i=1}^{N_2}$  respectively ( $N_1$  and  $N_2$  being the dimension of  $X_h$  and  $M_h$ ). The coordinates of the discrete unknowns  $v_h$ ,  $p_h$  and  $\eta_h^l$  in the bases  $B_{N_1}$  and  $B_{N_2}$  are  $[V_h] = (V_1, \dots, V_{N_1})$ ,  $[P_h] = (P_1, \dots, P_{N_2})$  and  $[(H_h)_l] = ((H_1)_l, \dots, (H_{N_2})_l)$ . In these bases, the semi-discretisation in the space of problem (24) can be written as,

$$\left\{ \begin{array}{l} (V_h, P_h, H_h) \in L^2(0, T; \mathbb{R}^{N_1}) \times L^2(0, T; \mathbb{R}^{N_2}) \times L^2(0, T; (\mathbb{R}^{N_2})^L) \text{ s.t. :} \\ M_v \frac{dV_h}{dt} + B_h P_h = F_h, \\ M_p \frac{dP_h}{dt} - \sum_{l=1}^L M_p \frac{d(H_h)_l}{dt} - B_h^T V_h = 0, \\ M_y^l \frac{d(H_h)_l}{dt} + M_\omega^l (H_h)_l - B_h^T V_h = 0, \forall l, \end{array} \right. \quad (25)$$

with

$$\begin{aligned} (M_v)_{ij} &= (\rho \mathbf{w}_i, \mathbf{w}_j), \quad \forall i, j = 1, \dots, N_1 \\ (M_p)_{ij} &= \left( \frac{1}{\mu_R} q_i, q_j \right), \quad \forall i, j = 1, \dots, N_2 \\ (M_y^l)_{ij} &= \left( \frac{1}{\mu_{Ry}^l} q_i, q_j \right), \quad \forall i, j = 1, \dots, N_2 \\ (M_\omega^l)_{ij} &= \left( \frac{\omega_l}{\mu_{Ry}^l} q_i, q_j \right), \quad \forall i, j = 1, \dots, N_2 \\ (B_h)_{ij} &= (\operatorname{div} w_i, q_j), \quad \forall i = 1, \dots, N_1, \quad j = 1, \dots, N_2 \end{aligned}$$

and where  $B_h^T$  denotes the transpose of  $B_h$ . In practice, we only consider regular domains in  $\mathbb{R}^d$ ,  $d = 1, 2$  that can be discretised with a uniform mesh  $\mathcal{T}_h$  composed by segments or squares of size  $h$ , depending on the dimension of the problem. The finite element spaces we use are

$$X_h = \left\{ \mathbf{w}_h \text{ in } X / \forall K \in \mathcal{T}_h, \mathbf{w}_h|_K \in (Q_1)^d \right\},$$

and

$$M_h = \left\{ q_h \in L^2 / \forall K \in \mathcal{T}_h, q_h|_K \in P_0(K) \right\}.$$

This mixed finite element was introduced in <sup>28</sup> and is illustrated in Figure 6. In this case, the degrees of freedom for the velocity, or in other words the elements of  $V_h$ , correspond to the nodal values of the velocity components. More precisely, because the velocity is not continuous we have two values for each component associated to each node. For  $v_x$

at node  $(i, j)$  for example, we have  $(v_x)_{ij}^u$  corresponding to the limit of the value from above  $((v_x)_{ij}^u = \lim_{\epsilon \rightarrow 0} (v_x)(x_i, y_j + \epsilon))$  and  $v_x^d$  corresponding to the limit of the value from below  $((v_x)_{ij}^d = \lim_{\epsilon \rightarrow 0} (v_x)(x_i, y_j - \epsilon))$ . The degrees of freedom for the pressure field and the memory variable in  $M_h$  correspond to their element values (i.e., the average of the function over the element). When coupled with the fictitious domain method, this choice of

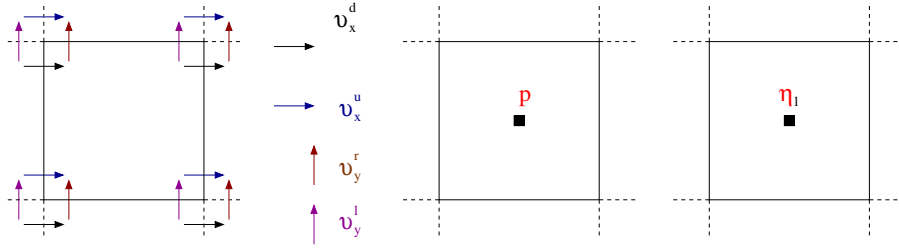


Fig. 6. Finite element  $v_h \in X_h, (p_h, (\eta_l)_h) \in M_h \times M_h$

finite elements presents some inconveniences. In particular, for the acoustic wave equation problem we cannot prove the convergence of the method from the theoretical point of view. Moreover, numerical results show that the method converges under restrictive conditions on the discretisation parameters. Thus, when the method is coupled with the fictitious domains, we replace  $M_h$  by  $M_h^1$  defined by,

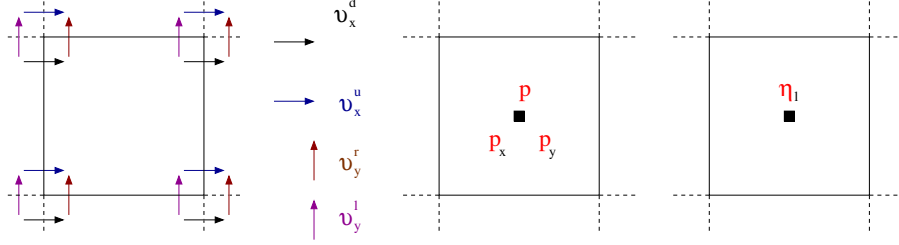
$$M_h^1 = \{q_h \in L^2 / \forall K \in \mathcal{T}_h, q_h|_K \in P_1(K)\}.$$

This finite element is presented Figure 7. In this case the degrees of freedom are the element values of the pressure field and its derivatives  $(p, \partial_x p, \partial_y p)$  <sup>(30)</sup>. The convergence of the method with this choice of discretisation spaces coupled with the fictitious domains is studied in <sup>30</sup> for the acoustic problem.

For computational reasons, however, it is natural to seek a discretisation which uses the least number of variables. In the proposed scheme pressure is thus discretised on the space  $M_h^1$  and the memory variables  $\eta_l$  are discretised on  $M_h$ . The semi-discretisation of the problem (24) in this case is, ( $N_3$  being the dimension of  $M_h^1$ )

$$\begin{cases} (V_h, P_h, H_h) \in L^2(0, T; \mathbb{R}^{N_1}) \times L^2(0, T; \mathbb{R}^{N_3}) \times L^2(0, T; (\mathbb{R}^{N_2})^L) \text{ s.t. :} \\ M_v \frac{dV_h}{dt} + B_h^1 P_h = F_h, \\ M_p^1 \frac{dP_h}{dt} - \sum_{l=1}^L M_p \frac{d(H_h)_l}{dt} - B_h^{1,T} V_h = 0, \\ M_y^l \frac{d(H_h)_l}{dt} + M_\omega^l (H_h)_l - B_h^T V_h = 0, \forall l, \end{cases} \quad (26)$$

where we introduced superscript 1 to indicate the matrices that involve the discretisation space  $M_h^1$ . In both cases (pressure discretised on  $M_h$  or  $M_h^1$ ), we use a second order centered


 Fig. 7. Finite element  $v_h \in X_h, (p_h, (\eta)_h) \in M_h^1 \times M_h$ 

finite difference scheme for the discretisation in time (here presented in the more general case with the pressure discretised on  $M_h^1$ ),

$$\left\{ \begin{array}{l} (V_h^{n+1}, P_h^{n+\frac{3}{2}}, H_h^{n+\frac{3}{2}}) \in \mathbb{R}^{N_1} \times \mathbb{R}^{N_3} \times (\mathbb{R}^{N_2})^L, \\ M_v \frac{V_h^{n+1} - V_h^n}{\Delta t} + B_h^1 P_h^{n+\frac{1}{2}} = (F_h)^{n+1/2}, \\ M_p^1 \frac{P_h^{n+\frac{3}{2}} - P_h^{n+\frac{1}{2}}}{\Delta t} - \sum_{l=1}^L M_p \frac{(H_h)_l^{n+\frac{3}{2}} - (H_h)_l^{n+\frac{1}{2}}}{\Delta t} - B_h^{1,T} V_h^{n+1} = 0, \\ M_y^l \frac{(H_h)_l^{n+\frac{3}{2}} - (H_h)_l^{n+\frac{1}{2}}}{\Delta t} + M_\omega^l \frac{(H_h)_l^{n+\frac{3}{2}} + (H_h)_l^{n+\frac{1}{2}}}{2} - B_h^T V_h^{n+1} = 0, \forall l. \end{array} \right. \quad (27)$$

The numerical scheme (27) becomes explicit in time when an adequate quadrature formula is used to approximate the matrix  $M_v$ . Note that the other mass matrices ( $M_p$ ,  $M_p^1$ ,  $M_y^l$ , and  $M_\omega^l$ ) are diagonal, since the spaces  $M_h$  and  $M_h^1$  are composed of discontinuous functions. For more details on the quadrature formulas used we refer the reader to <sup>28</sup>.

## 6. Stability and dispersion analysis

For the continuous problem, the energy is defined by

$$\varepsilon = \frac{1}{2} (\rho \mathbf{v}, \mathbf{v}) + \frac{1}{2} \left( p - \sum_{l=1}^L \eta_l, p - \sum_{l=1}^L \eta_l \right) + \sum_{l=1}^L \frac{1}{2y_l \mu_R} (\eta_l, \eta_l). \quad (28)$$

This quantity is positive (for  $y_l$  positive) and we have,

$$\frac{\partial \varepsilon}{\partial t} = - \sum_{l=1}^L \frac{w_l}{\mu_R y_l} \|\eta_l\|^2 \leq 0. \quad (29)$$

That is, the energy decreases as a function of time, which expresses the dissipative nature of the problem.

In the discrete case a stability analysis based on energy techniques permits us to show that the discrete scheme is stable under the following CFL condition (in homogeneous media

and for both choices  $M_h$  and  $M_h^1$  for the pressure discretisation),

$$\frac{\Delta t^2}{4} \frac{\mu_R}{\rho} \|B_h\|^2 \left(1 + \sum_{l=1}^L y_l\right) \leq 1, \quad (30)$$

with  $\|B_h^T B_h\| \geq \frac{4}{h^2}$  in 1D and  $\|B_h^T B_h\| \geq \frac{8}{h^2}$  in 2D. Note that these are the usual CFL conditions obtained in the non-dissipative case multiplied by  $\left(1 + \sum_{l=1}^L y_l\right)$ .

Furthermore, the dispersion relation also presents a similar aspect. For the the continuous problem we have,

$$\omega^2 = k^2 c^2 \left(1 + \sum_{l=1}^L \frac{\mathbf{i}\omega y_l}{\mathbf{i}\omega + \omega_l}\right). \quad (31)$$

For the discrete problem in 1D we obtain,

$$\sin^2\left(\frac{\omega \Delta t}{2}\right) = \frac{\Delta_t^2 c^2}{h^2} \left(\sin^2\left(\frac{kh}{2}\right)\right) \left(1 + \sum_{l=1}^L \frac{2\mathbf{i}y_l \tan\left(\frac{\omega \Delta t}{2}\right)}{\Delta_t \omega_l + 2\mathbf{i} \tan\left(\frac{\omega \Delta t}{2}\right)}\right), \quad (32)$$

and in 2D we get (for both choices  $M_h$  and  $M_h^1$  of the pressure discretisation),

$$\sin^2\left(\frac{\omega \Delta t}{2}\right) = \frac{\Delta_t^2 c^2}{h^2} \left(\sin^2\left(\frac{k_x h}{2}\right) + \sin^2\left(\frac{k_y h}{2}\right)\right) \left(1 + \sum_{l=1}^L \frac{2\mathbf{i}y_l \tan\left(\frac{\omega \Delta t}{2}\right)}{\Delta_t \omega_l + 2\mathbf{i} \tan\left(\frac{\omega \Delta t}{2}\right)}\right). \quad (33)$$

In figures 6 we have plotted the dispersion and attenuation curves as function of  $1/N$  ( $N$  being the number of points per wavelength used in the discretisation) for a plane incident wave, whose incident angle is 0 or  $\frac{\pi}{4}$  for the 2D case. Demonstration and details of the calculations for the stability and the dispersion relations for the discrete problem are exposed in the Appendix A and B.

## 7. The fictitious domain method

To model the free-surface boundary condition on the surface of the earth we use the fictitious domain method which has been developed for solving problems involving complex geometries<sup>34,12,13,14,15</sup>, and in particular for wave propagation problems<sup>16,17,18,19</sup>.

We follow here the approach proposed in<sup>19</sup>. Consider the viscoacoustic wave propagation problem in a domain with a complex geometry such as the one described in Figure 9. The

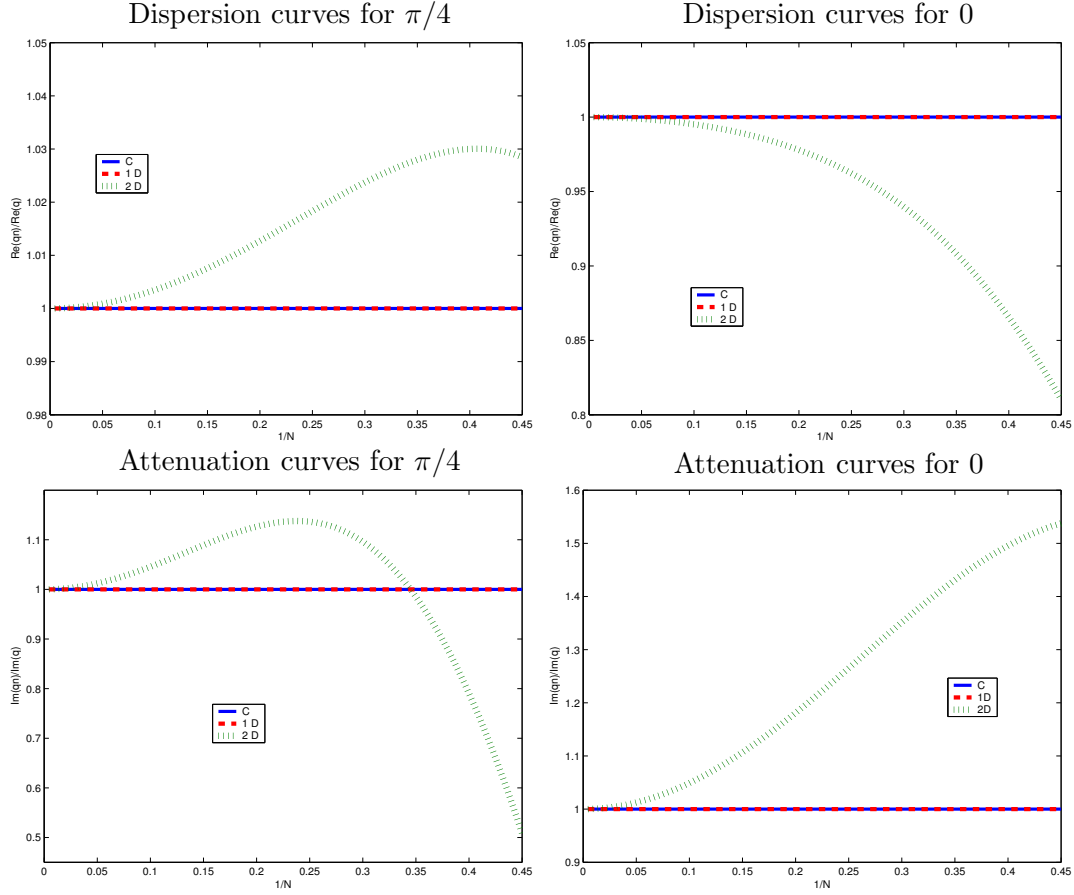


Fig. 8. Dispersion and attenuation curves for a plane incident wave, with incident angle 0 or  $\pi/4$  for the 1D and the 2D case ( $L = 3$ ).

initial problem is posed in  $\Omega$  with the free-surface boundary condition,  $\mathbf{v} \cdot \mathbf{n} = 0$  on  $\Gamma$ ,

$$\left\{ \begin{array}{ll} \rho \frac{\partial \mathbf{v}}{\partial t} - \nabla p = \mathbf{f} & \text{in } \Omega, \\ \frac{\partial p}{\partial t} - \sum_{l=1}^L \frac{\partial \eta_l}{\partial t} = \mu_R \operatorname{div}(\mathbf{v}) & \text{in } \Omega, \\ \frac{\partial \eta_l}{\partial t} + \omega_l \eta_l = \mu_R y_l \operatorname{div}(\mathbf{v}), \forall l & \text{in } \Omega, \\ \mathbf{v} \cdot \mathbf{n} = 0, & \text{on } \Gamma, \\ p = 0, & \text{on } \Gamma_D. \end{array} \right. \quad (34)$$

The main idea of the fictitious domain method is to extend the solution to a domain with a simple shape, independent of the complex geometry of the boundary, and to impose the boundary condition in a weak manner by introducing a Lagrange multiplier. Following this

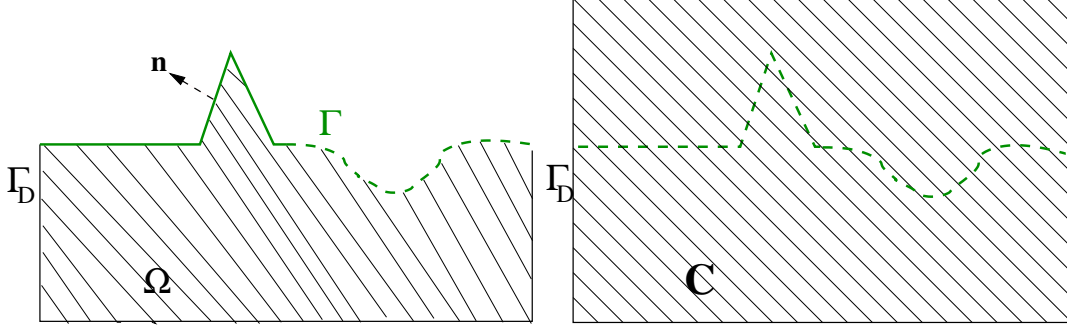


Fig. 9. Geometry of the problem: on the left the initial domain  $\Omega$  and on the right the extended domain  $C$ .

idea, we extend the solution  $(\mathbf{v}, p, \eta_l)$  by zero in the domain  $C$  (which is here a rectangle, see Figure 9). We denote  $(\tilde{\mathbf{v}}, \tilde{p}, \tilde{\eta}_l)$  the extended solution and have,

$$[\tilde{\mathbf{v}}\mathbf{n}]_{\Gamma} = 0 \Rightarrow \tilde{\mathbf{v}} \in H(\text{div}, C), [\tilde{p}]_{\Gamma} \neq 0, [\tilde{\eta}_l]_{\Gamma} \neq 0.$$

Thus, system (34) for the extended solution, can be written (in the distributional sense),

$$\left\{ \begin{array}{l} \rho \frac{\partial \tilde{\mathbf{v}}}{\partial t} - \nabla \tilde{p} = \mathbf{f} + [\tilde{p}]\mathbf{n}\delta_{\Gamma} \quad \text{in } C, \\ \frac{\partial \tilde{p}}{\partial t} - \sum_{l=1}^L \frac{\partial \tilde{\eta}_l}{\partial t} = \mu_R \text{div}(\tilde{\mathbf{v}}) \quad \text{in } C, \\ \frac{\partial \tilde{\eta}_l}{\partial t} + \omega_l \tilde{\eta}_l = \mu_{Rl} \text{div}(\tilde{\mathbf{v}}), \forall l \text{ in } C, \\ \tilde{\mathbf{v}} \cdot \mathbf{n} = 0, \quad \text{on } \Gamma, \\ p = 0, \quad \text{on } \Gamma_D. \end{array} \right. \quad (35)$$

In (35) we have two types of unknowns, the extended unknowns, defined in the simple shape domain  $C$  and the auxiliary variable  $[\tilde{p}]$ , defined on the boundary  $\Gamma$ . We introduce  $\lambda = [\tilde{p}]$  as a new unknown defined on  $\Gamma$ . This unknown can be interpreted as a Lagrange multiplier associated with the boundary condition on  $\Gamma$ . The variational formulation of the problem can then be written as follows,

$$\left\{ \begin{array}{l} \text{Find } (\mathbf{v}, p, H, \lambda) : ]0, T[ \rightarrow H(\text{div}; C) \times L^2(C) \times (L^2(C))^L \times H^{1/2}(\Gamma) \text{ s.t.} \\ \frac{d}{dt}(\rho \mathbf{v}, \mathbf{w}) + b(\mathbf{w}, p) - b_\Gamma(\lambda, \mathbf{w}) = (\mathbf{f}, \mathbf{w}), \quad \forall \mathbf{w} \in H(\text{div}; C), \\ \frac{d}{dt}\left(\frac{1}{\mu_R} p, q\right) - \sum_{l=1}^L \frac{d}{dt}\left(\frac{1}{\mu_R} \eta_l, q\right) - b(\mathbf{v}, q) = 0, \quad \forall q \in L^2(C), \\ \frac{d}{dt}\left(\frac{1}{\mu_{R\gamma_l}} \eta_l, q\right) + \left(\frac{\omega_l}{\mu_{R\gamma_l}} \eta_l, q\right) - b(\mathbf{v}, q) = 0, \quad \forall l, \quad \forall q \in L^2(C), \\ b_\Gamma(\mu, \mathbf{v}) = 0, \quad \forall \mu \in H^{1/2}(\Gamma), \end{array} \right.$$

where

$$b_\Gamma(\mu, \mathbf{w}) = \int_\Gamma \mu \mathbf{w} \cdot \mathbf{n} ds, \quad \forall (\mu, \mathbf{w}) \in H^{1/2}(\Gamma) \times H(\text{div}; C).$$

For the discretisation of this problem we consider a structured volume mesh  $\mathcal{T}_h$  on  $C$ , and an irregular surface mesh  $\mathcal{G}_{h_s}$  on  $\Gamma$ . The main advantage of this formulation is that the mesh for computing the extended functions can now be regular while the surface mesh is irregular and permits a good and efficient approximation of the geometry (see Figure 10).

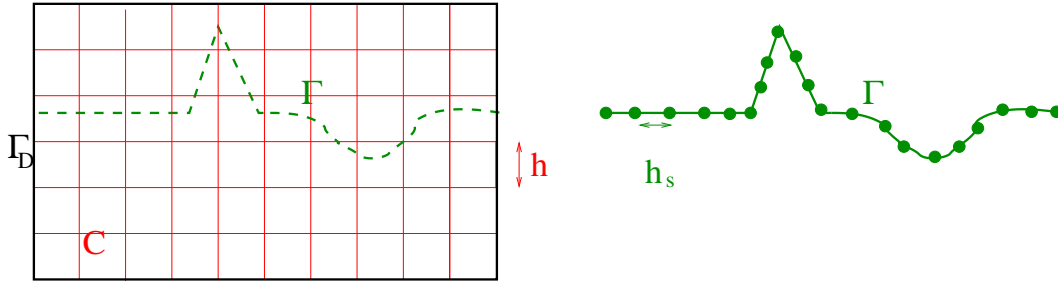


Fig. 10. The two meshes used in the fictitious domain method: a structured volume mesh on the domain  $C$  and an irregular surface mesh on  $\Gamma$ .

To discretise the volume unknowns  $(\mathbf{v}, p, H)$  we use the finite element method described in section 6 while for the Lagrange multiplier  $\lambda$  we use piecewise linear continuous functions on  $\mathcal{G}_{h_s}$ , i.e., the approximation space is,

$$G_{h_s} = \left\{ \mu_{h_s} \in H^{1/2}(\Gamma) / \forall S(\text{segment}) \in \mathcal{G}_{h_s}, \mu_{h_s}|_S \in P_1(S) \right\}.$$

To simplify the presentation, we considered in system (34) the homogeneous Dirichlet boundary condition on the boundary  $\Gamma_D$ . When the domain is infinite we use the perfectly matched layer model which will be described in the following section.

## 8. The PML method

The perfectly Matched Layer model was introduced by Bérenger<sup>20,21</sup> for Maxwell's equations and is now the most widely-used method for simulating wave propagation in unbounded domains. The reader can refer to<sup>22,23,24</sup> for electromagnetic waves, to<sup>25</sup> for anisotropic acoustic waves and to<sup>27,25</sup> for elastic waves. The popularity of this model is due to its simplicity and efficiency. Its most astonishing property is that for the continuous problem the reflection coefficient at the interface between the layer and the free medium is zero for all frequencies and angles of incidence. To derive the PML for the viscoacoustic

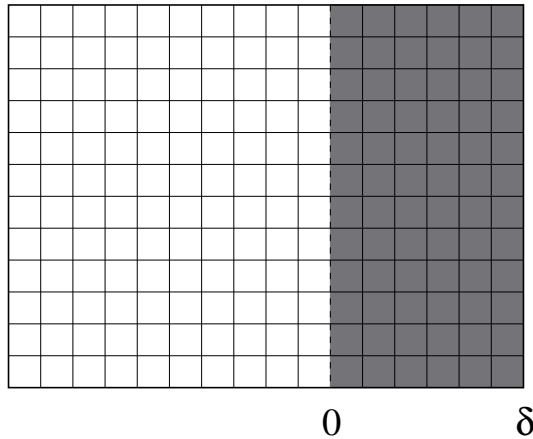


Fig. 11. PML in the  $x$ -direction: the physical medium is on the left and the absorbing medium is a layer of width  $\delta$ .

system (23) we follow the approach proposed in<sup>27</sup> which applies to any first-order linear hyperbolic system. We present here the construction of a PML in the  $x$ -direction (see Figure 11). Deriving then the PML for the other boundaries and the corners of the computational domain is a straightforward application of the same technique.

Following<sup>27</sup> we construct the PML model in two steps: (i) We split the solution  $(\mathbf{v}, p, \{\eta_l\})$  into two parts  $(\mathbf{v}^{\parallel}, p^{\parallel}, \{\eta_l^{\parallel}\})$  and  $(\mathbf{v}^{\perp}, p^{\perp}, \{\eta_l^{\perp}\})$ , with the parallel part being associated with the derivatives in the  $y$ -direction (direction parallel to the interface between the PML and the physical medium), and the orthogonal part associated with those in the  $x$ -direction. (ii) We introduce damping only on the orthogonal component of the solution.

When applying the splitting step to (23) by remarking that  $\mathbf{v}^{\parallel} = (0, v_y)$  and  $\mathbf{v}^{\perp} = (v_x, 0)$ ,

22 *J.-P. GROBY and C. TSOGKA*

we obtain,

$$\begin{cases} \rho \frac{\partial v_y}{\partial t} = \frac{\partial p}{\partial y} \\ \frac{\partial p^\parallel}{\partial t} - \sum_{l=1}^L \frac{\partial \eta_l^\parallel}{\partial t} = \mu_R \frac{\partial v_y}{\partial y} \\ \frac{\partial \eta_l^\parallel}{\partial t} + \omega_l \eta_l^\parallel = \mu_{Ryl} \frac{\partial v_y}{\partial y}, \end{cases} \quad (36)$$

and

$$\begin{cases} \rho \frac{\partial v_x}{\partial t} = \frac{\partial p}{\partial x} \\ \frac{\partial p^\perp}{\partial t} - \sum_{l=1}^L \frac{\partial \eta_l^\perp}{\partial t} = \mu_R \frac{\partial v_x}{\partial x} \\ \frac{\partial \eta_l^\perp}{\partial t} + \omega_l \eta_l^\perp = \mu_{Ryl} \frac{\partial v_x}{\partial x}, \end{cases} \quad (37)$$

with

$$\begin{cases} p = p^\parallel + p^\perp \\ \eta_l = \eta_l^\parallel + \eta_l^\perp, \forall l. \end{cases} \quad (38)$$

To apply the damping on the orthogonal components it is simpler to consider system (37) in the frequency domain. Then the PML consists in replacing the  $x$ -derivatives  $\partial_x$  by  $\frac{i\omega}{i\omega + d(x)}\partial_x$  (cf. <sup>27</sup>). Following this approach, system (37) in the frequency domain becomes,

$$\begin{cases} (i) \quad \rho(i\omega + d(x))v_x = \frac{\partial p}{\partial x} \\ (ii) \quad (i\omega + d(x))p^\perp - \sum_{l=1}^L (i\omega + d(x))\eta_l^\perp = \mu_R \frac{\partial v_x}{\partial x} \\ (iii) \quad (i\omega)(i\omega + d(x))\eta_l^\perp + (i\omega + d(x))\omega_l \eta_l^\perp = (i\omega)\mu_{Ryl} \frac{\partial v_x}{\partial x}, \end{cases} \quad (39)$$

where  $d(x)$  is the damping parameter which is equal to zero in the physical medium and non-negative in the absorbing medium.

We now introduce new variables  $\tilde{\eta}_l$  defined by,

$$i\omega \tilde{\eta}_l = (i\omega + d(x))\eta_l^\perp, \quad \forall l, \quad (40)$$

or equivalently in time domain,

$$\frac{\partial \tilde{\eta}_l}{\partial t} = \frac{\partial \eta_l^\perp}{\partial t} + d(x)\eta_l^\perp, \quad \forall l.$$

Using (40) in (39) and going in the time domain we get,

$$\begin{cases} \rho \frac{\partial v_x}{\partial t} + \rho d(x)v_x = \frac{\partial p}{\partial x} \\ \frac{\partial p^\perp}{\partial t} + d(x)p^\perp - \sum_{l=1}^L \frac{\partial \tilde{\eta}_l}{\partial t} = \mu_R \frac{\partial v_x}{\partial x} \\ \frac{\partial \tilde{\eta}_l}{\partial t} + \omega_l \tilde{\eta}_l = \mu_R y_l \frac{\partial v_x}{\partial x}. \end{cases} \quad (41)$$

The final system of equations for the PML is (41) together with (36), with  $p$  being defined by  $p = p^\parallel + p^\perp$ . Note that the memory variables  $\eta_l$  do not appear, and only the component  $\eta_l^\parallel$  and the variables  $\tilde{\eta}_l$  do appear, in this system.

Using a plane wave analysis, it can be shown (cf. <sup>27</sup>) that this model generates no reflection at the interface between the physical and the absorbing medium and that the wave decreases exponentially inside the layer. This property allows the use of a very high damping parameter inside the layer, and consequently of a small layer width, while achieving a near-perfect absorption of the waves. Note that for a finite-length absorbing layer there is some reflection due to the outer boundary of the PML.

**Remark 8.1.** To discretise the PML we use the same scheme as for the interior domain.

**Remark 8.2.** The damping  $d(x)$  is zero in the physical domain and non negative in the absorbing medium. In the numerical simulations it is defined as in <sup>27</sup>,

$$d(x) = \begin{cases} 0 & \text{for } x < 0 \\ \log\left(\frac{1}{R}\right) \frac{(n+1)\sqrt{\frac{\mu_R}{\rho}}}{2\delta} \left(\frac{x}{\delta}\right)^n & \text{for } x \geq 0 \end{cases} \quad (42)$$

where  $R$  is the theoretical reflection coefficient,  $\delta$  the width of the PML and  $n = 4$ .

In practice, we take  $R = 5.0 \cdot 10^{-7}$ , and  $\delta \approx 30\Delta_x$  (depending on the wavelength).

## 9. Numerical results

### 9.1. Scattering from a circular cylinder

In order to validate the proposed numerical method we consider in this section the canonical problem of a plane wave (Ricker wavelet) striking a viscoacoustic homogeneous circular cylinder. The geometry of the problem is displayed in Figure 12. A homogeneous viscoacoustic circular cylinder of radius  $a$  (domain  $\Omega_2$ ) is surrounded by a homogeneous non-dissipative medium (domain  $\Omega_1$ ). We denote by  $\Gamma_1$  the interface between the two domains  $\Omega_1$  and  $\Omega_2$ . The physical characteristics of the media are  $\rho_1 = 1000\text{kg/m}^3$ ,  $c_1 = 1500\text{m/s}$ ,  $Q_1 = +\infty$  in  $\Omega_1$  and  $\rho_2 = 1800\text{kg/m}^3$ ,  $c_2 = 3050\text{m/s}$  and  $Q_2 = 30$  in  $\Omega_2$ . The source function used in this example is given by (18) with  $f_0 = 2.5\text{Hz}$ . For this problem, the solution can be computed by an analytical method described in what follows (here with the Fourier transform defined by  $p(\mathbf{x}, t) = \int_{-\infty}^{\infty} p(\mathbf{x}, \omega) \exp(-i\omega t) d\omega$ ,  $\forall t \in \mathbb{R}$ ).

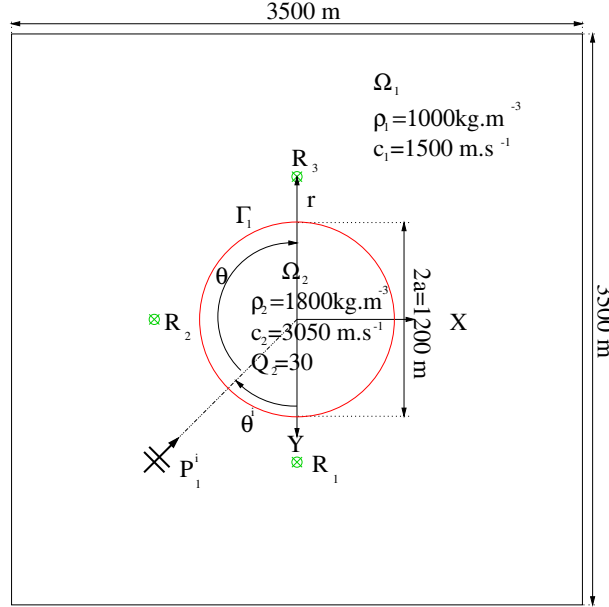


Fig. 12. The geometry of the problem: a homogeneous viscoacoustic cylinder of radius  $a$  (domain  $\Omega_2$ ) embedded in a non-dissipative homogeneous medium (domain  $\Omega_1$ ).

Consider the following incident plane wave (with incident angle  $0 \leq \theta^i < 2\pi$ ),

$$p_1^i(\mathbf{x}) = A_1^i \sum_{n=-\infty}^{n=\infty} e^{-in(\theta^i + \frac{\pi}{2})} J_n(k_1 r) \exp(i\mathbf{n}\theta); \quad \forall \mathbf{x} = (r \cos(\theta), r \sin(\theta)) \in \Omega_1. \quad (43)$$

Using the partial wave expansion we can express the solutions  $p_j \in \Omega_j, j = 1, 2$  in the following form,

$$\begin{aligned} p_1(\mathbf{x}) &= p_1^i(\mathbf{x}) + \sum_{n=-\infty}^{n=\infty} a_{1n} H_n^{(1)}(k_1 r) \exp(i\mathbf{n}\theta), \quad \forall \mathbf{x} \in \Omega_1 \\ p_2(\mathbf{x}) &= \sum_{n=-\infty}^{n=\infty} b_{2n} J_n(k_2(\omega) r) \exp(i\mathbf{n}\theta), \quad \forall \mathbf{x} \in \Omega_2, \end{aligned} \quad (44)$$

with  $H_n^{(1)}$  the first-kind Hankel function of order  $n$ ,  $J_n$  the Bessel function of order  $n$  and where the wave number in  $\Omega_2$  is computed by (3),

$$k_2(\omega) = k_2(\mathbf{x}, \omega) = \frac{\omega}{c_{ref}} \left( \frac{-i\omega}{\omega_{ref}} \right)^{-\frac{1}{\pi} \text{atan}(\frac{1}{Q_2})}; \quad \text{with } w_{ref} = 0.05. \quad (45)$$

To compute the coefficients  $a_{1n}$  and  $b_{2n}$  we introduce the expressions for  $p_1$  and  $p_2$ , i.e., equation (44) in the transmission boundary conditions on  $\Gamma_1$  (continuity of the pressure and the normal component of velocity). After projecting the resulting system onto the Fourier

basis  $\left(\frac{1}{2\pi}\exp(-im\theta); m \in \mathbf{Z}\right)$  we obtain,

$$\begin{aligned} a_{1n} &= \frac{\gamma_1 \dot{J}_n(\chi_1) J_n(\chi_2) - \gamma_2 J_n(\chi_1) \dot{J}_n(\chi_2)}{-\gamma_1 \dot{H}_n^{(1)}(\chi_1) J_n(\chi_2) + \gamma_2 \dot{J}_n(\chi_2) H_n^{(1)}(\chi_1)} A_1^i e^{-in(\theta^i + \frac{\pi}{2})} \\ b_{2n} &= \frac{\gamma_1 \dot{J}_n(\chi_1) H_n^{(1)}(\chi_1) - \gamma_1 J_n(\chi_1) \dot{H}_n^{(1)}(\chi_1)}{\gamma_2 \dot{J}_n(\chi_2) H_n^{(1)}(\chi_1) - \gamma_1 \dot{H}_n^{(1)}(\chi_1) J_n(\chi_2)} A_1^i e^{-in(\theta^i + \frac{\pi}{2})}, \end{aligned} \quad (46)$$

with  $\dot{Z}_n(z) = \frac{dZ_n(z)}{dz}$ ,  $\chi_j = k_j a$ , and  $\gamma_j = \frac{k_j}{\rho_j}$ . The insertion of these expressions into (44) gives the final solution of the problem<sup>35</sup>. Comparison of results between the analytical and the numerical solution are displayed in Figure 13 where we can see that good agreement is obtained between the two (the maximal relative error at  $R_1$  is 4%). In this computation the space discretization step is  $h = 5m$  and the time discretization step is chosen with respect to the CFL condition

$$\Delta t = \frac{\sqrt{2}h}{2c_{\max}}, \quad c_{\max} = \max\left(c_1, c_2 \sqrt{\left(1 + \sum_{l=1}^L y_l\right)}\right) = c_2 \sqrt{\left(1 + \sum_{l=1}^L y_l\right)},$$

where the  $y_l$ 's correspond to medium 2. In the numerical simulation, we assume that the

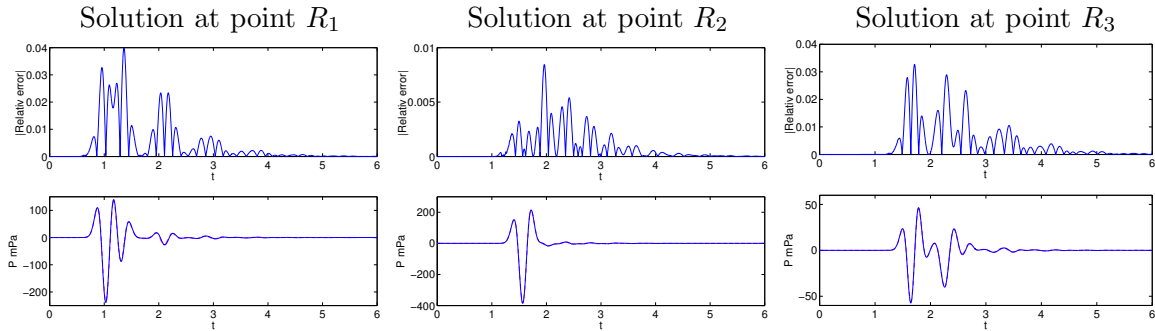


Fig. 13. Comparison between the analytical solution (dashed line) and the numerical solution (continuous line) at different observation points  $R_1$ ,  $R_2$  and  $R_3$ . The location of the observation points is illustrated in Figure 12. In the figures the x-axis is time (in s) and the y-axis is the pressure field.

problem is posed in the whole space and to solve it, we couple system (27) with the perfectly matched absorbing layer model (PML). To test numerically the convergence rate of the method we have carried out the following experiment. For different discretisation steps  $h = 25m$ ,  $10m$  and  $5m$  we compare the solution obtained numerically with the analytical one at the three observation points  $R_i$ ,  $i = 1, \dots, 3$ . More precisely, we introduce the following measure of the error,

$$E = \sqrt{\left(\sum_{R_1, R_2, R_3} \sum_t (P_{an} - P_{num})^2 dt\right)}. \quad (47)$$

In figure 14 we plot the logarithm of  $E$  as a function of the logarithm of the discretisation step  $h$ . The slope of the obtained curve gives us an indication of the convergence of the method (here the slope is 1.9). The convergence of the method when coupled with the

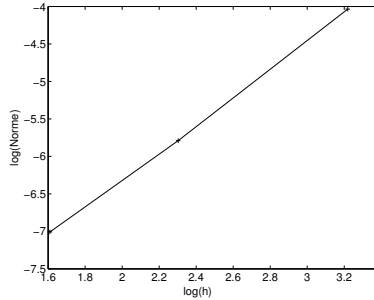


Fig. 14. The logarithm of  $E$  as a function of the logarithm of  $h$  ( $\log(E) = f(\log(h))$ ). The estimated slope is 1.9.

fictitious domains is addressed in <sup>30</sup>. In this case we observe numerically that the rate of convergence is lower in the vicinity of the boundary  $\Gamma$  on which the fictitious domain method is employed. This is intuitive as lower convergence rates are expected in the elements that  $\Gamma$  intersects, because the solution is less regular in those elements.

### 9.2. *Simulation of the response to an incident cylindrical wave of a dike on a flexible foundation embedded in a half-space*

To illustrate the efficiency of the method we model in this section the response to an incident cylindrical wave of a dike on a flexible foundation embedded in a half-space. This particular problem was considered in <sup>36</sup> where it was solved using an expansion of the solution in cylindrical wave functions in the case of non-dissipative media. In <sup>36</sup> the authors studied this problem for different material parameters in order to determine how stiff the foundation should be relative to the soil for the rigid foundation assumption in soil-structure interaction models to be valid. They concluded that a foundation with the same mass density as the soil but 50 times larger shear modulus behaves in rigid manner for this problem. However, for ratios of shear moduli less than 16, the rigid foundation assumption is not valid. In this case, soil-structure interaction models with a rigid-foundation assumption will not model the differential motion of the ground and may underestimate the stresses in the structure (cf. <sup>36</sup>). We consider here a ratio of shear moduli equal to 4. Soil-structure interaction is taken into account owing to the fact that we discretise the continuous problem.

The pulse associated with the incident wave is created by a line source of the form,

$$g(\mathbf{x}, t) = \frac{df(t)}{dt} \left( 1 - \frac{r^2}{r_s^2} \right) 1_{B_s}, \quad (48)$$

with  $f(t)$  defined by (18) and where  $r$  is the radius coordinate in the sagitale plane.  $1_{B_s}$  is the characteristic function of the disc  $B_s$  centered at  $\mathbf{x}_s$  (location of the source) and

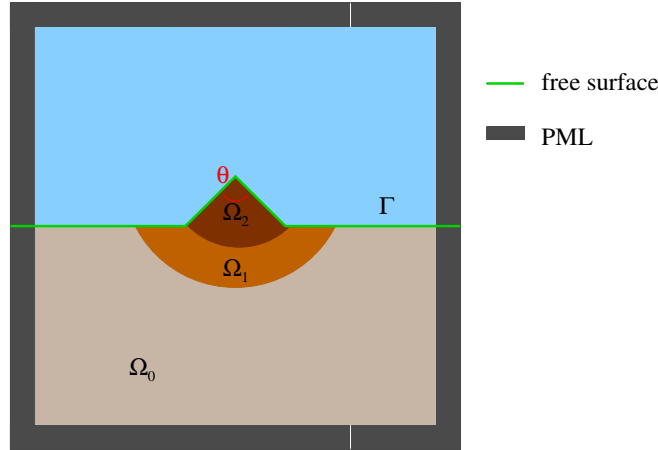


Fig. 15. The geometry of the problem: a dike on a flexible foundation embedded in a half-space.

with radius  $r_s$ . In (48), the function multiplying  $\frac{df(t)}{dt}$  is a smooth approximation of the delta function  $\delta(r)$ . The radius  $r_s$  is small, typically equal to a few discretisation steps. The geometry of the problem is illustrated in Figure 15, where  $\Gamma$  denotes the free surface,  $\Omega_0$  the hard bedrock,  $\Omega_1$  the flexible foundation and  $\Omega_2$  the dike. The physical parameters used in the simulation are  $\rho_0 = 1000\text{kg/m}^3$ ,  $c_0 = 1450\text{m/s}$ ,  $Q_0 = +\infty$  in the bedrock,  $\rho_1 = 1000\text{kg/m}^3$ ,  $c_1 = 2900\text{m/s}$ ,  $Q_1 = 30$  in  $\Omega_1$  and  $\rho_2 = 250\text{kg/m}^3$ ,  $c_2 = 725\text{m/s}$ ,  $Q_2 = 100$  in the dike. The angle  $\theta$  is equal to  $\pi/2$ .

In Figure 16 we display snapshots of the solution (the pressure field) at different times. Diffraction from the free surface is modeled by embedding the solution in a domain of a simple shape using the fictitious domain method. To model wave propagation in the infinite half-space the fictitious domain is surrounded by an absorbing medium using the PML model. Although for this problem a semi-analytical method similar to the one used in <sup>36</sup> can be employed to compute the solution, the numerical method proposed in this paper is more general in that it can be applied to any complicated geometry and/or propagation media. Moreover, our numerical method can be of particular interest in cases where the rigid foundation assumption is not valid as it can provide realistic values for the stresses in the structure.

## Conclusion

We employed a rational approximation of the frequency-dependent viscoacoustic modulus in order to introduce dissipation into time-domain computations. To do so, we followed the approach in <sup>3</sup> and chose relaxation frequencies  $w_l(\mathbf{x})$  equidistant on a logarithmic scale in the frequency range  $[\frac{w_{max}}{100}; w_{max}]$ , where  $w_{max}$  is the maximal frequency of the used source spectrum. This approach will be accurate for propagation in media with a quality factor greater than 10. For media with high attenuation ( $Q < 10$ ) it is necessary in order to obtain accurate results to use a non-linear minimization method such as the one proposed in <sup>8</sup>.

By introducing this approximation of the viscoacoustic modulus into the velocity-

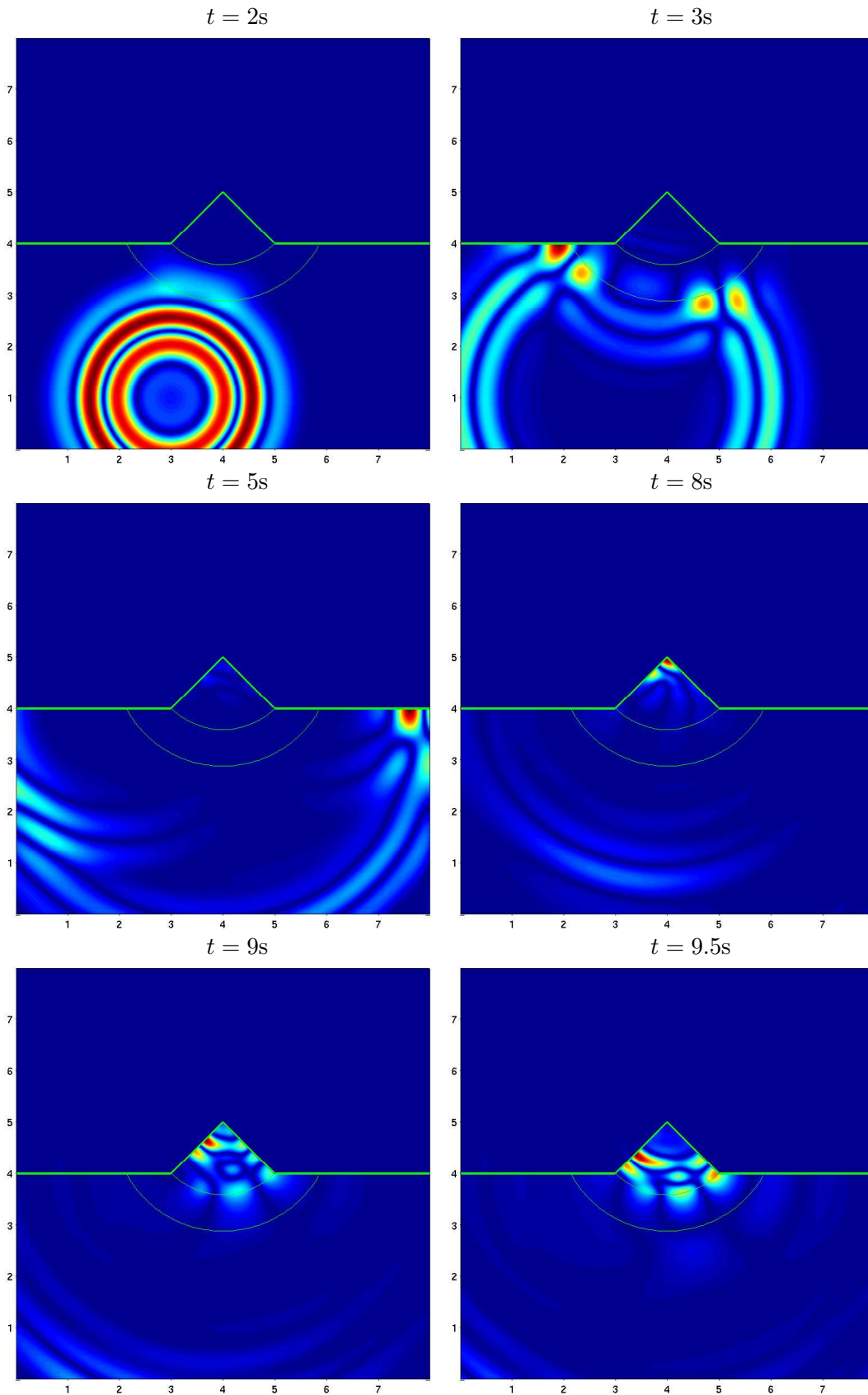


Fig. 16. Snapshots of the solution: the pressure field in the computational domain at different times

pressure formulation we obtained a first-order- in-time linear system of equations. To discretise this system we used a mixed finite-element method for the discretisation in space and a second-order finite difference scheme in time.

The velocity-pressure formulation was coupled with the fictitious domain method in order to model the free surface boundary condition on boundaries with complicated geometries, and with the PML method to simulate wave propagation in unbounded domains. The efficiency of the method was illustrated by numerical results.

## Appendix

### A. Stability analysis

#### A.1. The continuous problem

We rewrite the continuous system in time with zero source term,

$$\rho \frac{\partial \mathbf{v}}{\partial t} = \nabla p, \quad (\text{A.1})$$

$$\frac{\partial p}{\partial t} - \sum_{l=1}^L \frac{\partial \eta_l}{\partial t} = \mu_R \operatorname{div}(\mathbf{v}), \quad (\text{A.2})$$

$$\frac{\partial \eta_l}{\partial t} + \omega_l \eta_l = \mu_R y_l \operatorname{div}(\mathbf{v}), \forall l. \quad (\text{A.3})$$

By taking the inner products (in  $L^2$ ) of (A.1) with  $\mathbf{v}$ , (A.2) with  $\left(p - \sum_{l=1}^L \eta_l\right)$ , and (A.2) with  $\eta_l$  we get

$$\left(\rho \frac{\partial \mathbf{v}}{\partial t}, \mathbf{v}\right) = (\nabla(p), \mathbf{v}), \quad (\text{A.4})$$

$$\left(\frac{\partial}{\partial t} \left(p - \sum_{l=1}^L \eta_l\right), \left(p - \sum_{l=1}^L \eta_l\right)\right) = \mu_R \left(\operatorname{div}(\mathbf{v}), \left(p - \sum_{l=1}^L \eta_l\right)\right), \quad (\text{A.5})$$

$$\left(\frac{\partial \eta_l}{\partial t}, \eta_l\right) + (\omega_l \eta_l, \eta_l) = \mu_R y_l (\operatorname{div}(\mathbf{v}), \eta_l). \quad (\text{A.6})$$

Then, summing (A.4) +  $\frac{(A.5)}{\mu_R} + \sum_{l=1}^L \frac{(A.6)}{y_l \mu_R}$ , we obtain,

$$\left(\rho \frac{\partial v}{\partial t}, \mathbf{v}\right) + \frac{1}{\mu_R} \left(\frac{\partial}{\partial t} \left(p - \sum_{l=1}^L \eta_l\right), \left(p - \sum_{l=1}^L \eta_l\right)\right) + \sum_{l=1}^L \frac{1}{y_l \mu_R} \left(\frac{\partial \eta_l}{\partial t}, \eta_l\right) = - \sum_{l=1}^L \frac{\omega_l}{\mu_R y_l} (\eta_l, \eta_l) \quad (\text{A.7})$$

Keeping in mind that the energy of the system is,

$$\varepsilon = \frac{1}{2} (\rho \mathbf{v}, \mathbf{v}) + \frac{1}{2\mu_R} \left(\left(p - \sum_{l=1}^L \eta_l\right), \left(p - \sum_{l=1}^L \eta_l\right)\right) + \sum_{l=1}^L \frac{1}{2y_l \mu_R} (\eta_l, \eta_l) \quad (\text{A.8})$$

we finally get,

$$\frac{\partial \varepsilon}{\partial t} = - \sum_{l=1}^L \frac{\omega_l}{\mu_R y_l} \|\eta_l\|^2 \leq 0. \quad (\text{A.9})$$

Which implies that the energy of the system is decreasing with time, when  $\omega_l$ ,  $\mu_R$  and  $y_l$  are positive quantities. The relaxation frequencies  $\omega_l$  are always positive and the same holds for the relaxed modulus  $\mu_R$ . The coefficients  $y_l$  can in practice become negative if we do not

solve a constraint minimization problem. However, we never encountered in practice a case for which

$$-\sum_{l=1}^L \frac{\omega_l}{\mu_R y_l} \|\eta_l\|^2 \geq 0,$$

and thus the problem becomes unstable (in the sense that the energy increases). To avoid this instability a constraint minimization algorithm seeking for non-negative  $y_l$  can be used.

### A.2. The discrete problem

We consider here the more general case where the pressure field is discretised in  $M_h^1$ . Remark that the discretisation space  $M_h^1$  admits the following orthogonal decomposition in  $L^2$ ,

$$M_h^1 = M_h \oplus (M_h)^\perp,$$

where  $M_h$  is the space of piecewise constant functions,

$$M_h = \{q_h \in L^2 / \forall K \in \mathcal{T}_h, q_h|_K \in P_0(K)\},$$

and  $(M_h)^\perp$  is its orthogonal complement in  $M_h^1$  (with respect to the inner product in  $L^2$ ). So that for any  $p_h \in M_h^1$ , we can write  $p_h = p_h^0 + p_h^1$  with  $p_h^0$ , the projection of  $p_h$  on  $M_h$  and  $p_h^1$  the projection of  $p_h$  on  $(M_h)^\perp$ . Moreover, if  $P, P_0$  and  $P_1$  are the coordinates of  $p_h, p_h^0$  and  $p_h^1$  in the basis of  $M_h^1, M_h$  and  $(M_h)^\perp$ , then we have  $P = [P_0, P_1]$ . Note that the memory variables are only discretised on  $M_h$ . In this case, we can rewrite the discrete system as, (capital letters are used for the discrete unknowns and the subscript  $h$  is omitted)

$$\rho M_v \frac{V^{n+\frac{1}{2}} - V^{n-\frac{1}{2}}}{\Delta t} = -B_h^0 P_0^n - B_h^1 P_1^n \quad (\text{A.10})$$

$$M_0 \frac{P_0^{n+1} - P_0^n}{\Delta t} - M_0 \sum_{l=1}^L \frac{H_l^{n+1} - H_l^n}{\Delta t} = \mu_R B_h^{0,T} V^{n+\frac{1}{2}}, \quad (\text{A.11})$$

$$M_1 \frac{P_1^{n+1} - P_1^n}{\Delta t} = \mu_R B_h^{1,T} V^{n+\frac{1}{2}}, \quad (\text{A.12})$$

$$M_0 \frac{H_l^{n+1} - H_l^n}{\Delta t} + \omega_l M_0 \frac{H_l^{n+1} + H_l^n}{2} = \mu_R y_l B_h^{0,T} V^{n+\frac{1}{2}}, \quad (\text{A.13})$$

with

$$(M_v)_{ij} = (\mathbf{w}_i, \mathbf{w}_j), \quad \forall i, j, \text{ basis functions of } X_h,$$

$$(M_0)_{ij} = (q_i, q_j), \quad \forall q_i, q_j, \text{ basis functions of } M_h,$$

$$(M_1)_{ij} = (q_i, q_j), \quad \forall q_i, q_j, \text{ basis functions of } (M_h)^\perp.$$

Then considering the inner products  $((\text{A.10}) \text{ at time } (n+3/2) + ((\text{A.10}) \text{ at time } n+1/2)) \times V^{n+\frac{1}{2}}, (\text{A.11}) \times \left( P_0^{n+1} - \sum_{l=1}^L H_l^{n+1} + P_0^n - \sum_{l=1}^L H_l^n \right), (\text{A.12}) \times (P_1^{n+1} + P_1^n), \text{ and } (\text{A.13}) \times (H_l^{n+1} + H_l^n)$ , we get,

$$\begin{aligned} (\rho M_v V^{n+\frac{3}{2}}, V^{n+\frac{1}{2}}) &= (\rho M_v V^{n+\frac{1}{2}}, V^{n-\frac{1}{2}}) \\ &\quad - \Delta t (B_h^0(P_0^n + P_0^{n+1}), V^{n+\frac{1}{2}}) - \Delta t (B_h^1(P_1^n + P_1^{n+1}), V^{n+\frac{1}{2}}) \end{aligned} \quad (\text{A.14})$$

$$\begin{aligned} \|P_0^{n+1} - \sum_{l=1}^L H_l^{n+1}\|_{M_0}^2 &= \|P_0^n - \sum_{l=1}^L H_l^n\|_{M_0}^2 \\ &\quad + \Delta t \mu_R (B_h^{0,T} V^{n+\frac{1}{2}}, P_0^{n+1} + P_0^n) - \Delta t \mu_R \left( B_h^{0,T} V^{n+\frac{1}{2}}, \sum_{l=1}^L H_l^{n+1} + H_l^n \right) \end{aligned} \quad (\text{A.15})$$

$$\|P_1^{n+1}\|_{M_1}^2 = \|P_1^n\|_{M_1}^2 + \Delta t \mu_R (B_h^{1,T} V^{n+\frac{1}{2}}, P_1^{n+1} + P_1^n) \quad (\text{A.16})$$

$$\begin{aligned} \|H_l^{n+1}\|_{M_0}^2 &= \|H_l^n\|_{M_0}^2 \\ &\quad - \omega_l \Delta t \frac{\|H_l^{n+1} - H_l^n\|_{M_0}^2}{2} + \mu_R \Delta t y_l (B_h^{0,T} V^{n+\frac{1}{2}}, H_l^{n+1} + H_l^n) \end{aligned} \quad (\text{A.17})$$

where the norms  $\|\cdot\|_{M_0}$  and  $\|\cdot\|_{M_1}$  are defined by

$$\|q\|_{M_0}^2 = (M_0 q, q), \quad \|q\|_{M_1}^2 = (M_1 q, q),$$

Summing (A.14) +  $\frac{(A.15)}{\mu_R}$  +  $\frac{(A.16)}{\mu_R}$  +  $\sum_{l=1}^L \frac{(A.17)}{y_l \mu_R}$ , we get,

$$\frac{\varepsilon_h^{n+1} - \varepsilon_h^n}{\Delta t} = - \sum_{l=1}^L \frac{\omega_l}{\mu_R y_l} \frac{\|H_l^{n+1} + H_l^n\|_{M_0}^2}{4}, \quad (\text{A.18})$$

with the discrete energy being defined by,

$$2\varepsilon_h^n = (\rho M_v V^{n+\frac{1}{2}}, V^{n-\frac{1}{2}}) + \frac{1}{\mu_R} \|P_1^n\|_{M_1}^2 + \frac{1}{\mu_R} \|P_0^n - \sum_{l=1}^L H_l^n\|_{M_0}^2 + \sum_{l=1}^L \frac{\|H_l^n\|_{M_0}^2}{\mu_R y_l}. \quad (\text{A.19})$$

Equation (A.18) shows that the discrete energy is also decreasing, under the same assumptions on  $y_l$  as in A.1.

To show under which condition the quantity defined by (A.19) is positive and thus an energy, we use the orthogonal decomposition of  $M_h^1$  to get,

$$\begin{aligned} 2\varepsilon_h^n &= \frac{1}{4} (\rho M_v (V^{n+\frac{1}{2}} + V^{n-\frac{1}{2}}), (V^{n+\frac{1}{2}} + V^{n-\frac{1}{2}})) + \frac{\|P^n\|_M^2}{\mu_R} + \sum_{l=1}^L \frac{\|H_l^n\|_{M_0}^2}{\mu_R y_l} + \\ &\quad \frac{1}{\mu_R} \left( M_0 \sum_{l=1}^L H_l^n, \sum_{l=1}^L H_l^n \right) - \frac{2}{\mu_R} \left( DP^n, \sum_{l=1}^L H_l^n \right) - \frac{\Delta t^2}{4\rho} (B_h P^n, B_h P^n), \end{aligned} \quad (\text{A.20})$$

with

$$\begin{aligned} \|q\|_M^2 &\equiv (Mq, q) = (M_0q_0, q_0) + (M_1q_1, q_1), \\ (DP, H_l) &= (M_0P_0, H_l), \\ B_h P^n &= B_h^0 P_0^n + B_h^1 P_1^n. \end{aligned}$$

From (A.20) we obtain,

$$2\varepsilon_h^n \geq \frac{1}{\mu_R} \left[ \left( 1 - \frac{\Delta t^2 \mu_R \|B_h\|^2}{4\rho} \right) \|P^n\|_M^2 + \left\| \sum_{l=1}^L H_l^n \right\|_{M_0} - 2 \left( DP^n, \sum_{l=1}^L H_l^n \right) + \sum_{l=1}^L \frac{\|H_l^n\|_{M_0}^2}{y_l} \right]$$

with  $\|B_h\|^2 = \sup_P \frac{(B_h P, B_h P)}{(MP, P)}$ . We rewrite this equation as a matrix associated with the quadratic formulation and we prove that the eigenvalues of this matrix are positive under the CFL condition, (with  $\|B_h\|^2 \geq \frac{4}{h^2}$  in 1D and  $\|B_h\|^2 \geq \frac{8}{h^2}$  in 2D)

$$\frac{\Delta t^2 \mu_R}{4\rho} \|B_h\|^2 \left( 1 + \sum_{l=1}^L y_l \right) \leq 1.$$

## B. Dispersion analysis

### B.1. The continuous problem

Suppose that  $\mathbf{v}(\mathbf{x}, t)$ ,  $p(\mathbf{x}, t)$ , and  $\eta_l(\mathbf{x}, t) \forall l$ , are plane waves,

$$\begin{cases} \mathbf{v}(\mathbf{x}, t) = \mathbf{v}_0 \exp(\mathbf{i}(\omega t - \mathbf{K}\mathbf{x})), \\ p(\mathbf{x}, t) = p_0 \exp(\mathbf{i}(\omega t - \mathbf{K}\mathbf{x})), \\ \eta_l(\mathbf{x}, t) = \eta_l^0 \exp(\mathbf{i}(\omega t - \mathbf{K}\mathbf{x})), \end{cases}$$

$\mathbf{K}\mathbf{x} = kx$  in 1D and  $\mathbf{K}\mathbf{x} = k_x x + k_y y = k \cos(\Phi)x + k \sin(\Phi)y$ ,  $\Phi$  being the incident angle of the plane wave in 2D. Introducing this expression into (23), we get the dispersion relation,

$$\omega^2 = \mathbf{K}^2 c_R^2 \left( 1 + \sum_{l=1}^L \frac{\mathbf{i}\omega y_l}{\mathbf{i}\omega + \omega_l} \right) \quad (\text{B.1})$$

with  $c_R = \sqrt{\frac{\mu_R}{\rho}}$  the relaxed velocity. If the medium is non-dissipative (i.e.,  $y_l = 0 \forall l$ ), (B.1) becomes the well-known relation  $\omega^2 = \mathbf{K}^2 c^2$ . Note that the dispersion relation (B.1) is no longer explicit in  $\omega$ .

### B.2. The discrete problem

We are interested in the general formulation for which the pressure field is discretised in  $M_h^1$  and  $\eta_l$  in  $M_h$ . Considering that  $V$ ,  $P$ , and  $H_l$  are plane waves, and employing the same

34 *J.-P. GROBY and C. TSOGKA*

notation as in A.2, we get,

$$\sin^2(\chi_t) = \frac{\Delta t^2 c_R^2}{4} \left( B_h B_h^T + \sum_{l=1}^L B_h^0 B_h^{0,T} \frac{2i y_l \tan(\chi_t)}{\Delta t \omega_l + 2i \tan(\chi_t)} \right) \quad (\text{B.2})$$

where  $\chi_t = \frac{\omega \Delta t}{2}$ ,  $\Delta t$  being the time discretisation step. After some calculations we obtain,

$$\begin{aligned} \sin^2\left(\frac{\omega \Delta t}{2}\right) &= \frac{\Delta t^2 c_R^2}{h^2} \left( \sin^2\left(\frac{kh}{2}\right) \right) \left( 1 + \sum_{l=1}^L \frac{2i y_l \tan\left(\frac{\omega \Delta t}{2}\right)}{\Delta t \omega_l + 2i \tan\left(\frac{\omega \Delta t}{2}\right)} \right) && \text{in 1D} \\ \sin^2\left(\frac{\omega \Delta t}{2}\right) &= \frac{\Delta t^2 c_R^2}{h^2} \left( \sin^2\left(\frac{k_x h}{2}\right) + \sin^2\left(\frac{k_y h}{2}\right) \right) \left( 1 + \sum_{l=1}^L \frac{2i y_l \tan\left(\frac{\omega \Delta t}{2}\right)}{\Delta t \omega_l + 2i \tan\left(\frac{\omega \Delta t}{2}\right)} \right) && \text{in 2D} \end{aligned} \quad (\text{B.3})$$

wherein  $h$  is the discretisation step in space.

## References

1. W. I. Futterman. Dispersive body waves. *J. Geophys. Res.*, 67:5279–5291, 1962.
2. S.M. Day and J.B. Minster. Numerical simulation of attenuated wavefields using a pade approximant method. *Geophys. J. Roy. Astr. Soc.*, 78:105–118, 1984.
3. H. Emmerich and M. Korn. Incorporation of attenuation into time-domain computations of seismic wave fields. *Geophysics*, 52:1252–1264, 1987.
4. J. Carcione, D. Kosloff, and R. Kosloff. Viscoacoustic wave propagation simulation in the earth. *Geophysics*, 53:769–777, 1988.
5. J. O. Blanch, J.O.A Robertson, and W. W. Symes. Modeling of a constant  $q$ : Methodology and algorithm for an efficient and optimally inexpensive viscoelastic technique. *Geophysics*, 60:176–184, 1995.
6. J. Carcione, D. Kosloff, and R. Kosloff. Wave propagation simulation a linear viscoacoustic medium. *Geophys. J. R. astr. Soc.*, 93:393–407, 1988.
7. J. Carcione, D. Kosloff, and R. Kosloff. Wave propagation simulation a linear viscoelastic medium. *Geophys. J. R. astr. Soc.*, 95:597–611, 1988.
8. S. Asvadurov, L. Knizhnerman, and J. Pabon. Finite-difference modeling of viscoelastic materials with quality factors  $Q$  of arbitrary magnitude. *preprint*, 2003.
9. E. Bécache, A. Ezziani, and P. Joly. Mathematical and numerical modeling of wave propagation in linear viscoelastic media. In G.C. Cohen, E. Heikkola, P. Joly, and P. Neittaanmäki, editors, *Mathematical and Numerical Aspects of Wave Propagation*, pages 916–921. Springer, 2003.
10. V.K. Saul’ev. On solution of some boundary value problems on high performance computers by fictitious domain method. *Siberian Math. J.*, 4(4):912–925, 1963 (in Russian).
11. Q.V. Dihn, R. Glowinski, J. He, V. Kwock, T. W. Pan, and J. Périaux. Lagrange multiplier approach to fictitious domain methods: Application to fluid dynamics and electromagnetics. In D.E. Keyes, T.F. Chan, G.A. Meurant, J.S. Scroggs, and R.G. Voigt, editors, *Fifth International Symposium on Domain Decomposition Methods for Partial Differential Equations*, pages 151–154, Philadelphia, PA, 1992. SIAM.
12. R. Glowinski, T.W. Pan, and J. Periaux. A fictitious domain method for Dirichlet problem and applications. *Comp. Meth. in Appl. Mech. and Eng.*, pages 283–303, 1994.
13. R. Glowinski, T.W. Pan, and J. Periaux. A fictitious domain method for external incompressible viscous flow modeled by Navier-Stokes equations. *Comp. Meth. in Appl. Mech. and Eng.*, pages 283–303, 1994.

14. V. Girault and R. Glowinski. Error analysis of a fictitious domain method applied to a Dirichlet problem. *Japan J. Indust. Appl. Math.*, 12(3):487–514, 1995.
15. Roland Glowinski and Yuri Kuznetsov. On the solution of the Dirichlet problem for linear elliptic operators by a distributed Lagrange multiplier method. *C. R. Acad. Sci. Paris Sér. I Math.*, 327(7):693–698, 1998.
16. F. Collino, P. Joly, and F. Millot. Fictitious domain method for unsteady problems: Application to electromagnetic scattering. *J.C.P.*, 138(2):907–938, December 1997.
17. S. Garcès. *Application des méthodes de domaines fictifs à la modélisation des structures rayonnantes tridimensionnelles*. PhD thesis, ENSAE, 1998.
18. L. Rhaouti. *Domaines fictifs pour la modélisation d'un problème d'interaction fluide-structure: simulation de la timbale*. PhD thesis, Paris IX, 1999.
19. E. Bécache, P. Joly, and C. Tsogka. Fictitious domains, mixed finite elements and perfectly matched layers for 2d elastic wave propagation. *J. of Comp. Acous.*, 9(3):1175–1203, 2001.
20. J.P. Bérenger. A perfectly matched layer for the absorption of electromagnetic waves. *Journal of Comp. Physics.*, 114:185–200, 1994.
21. J.P. Bérenger. Three-dimensional perfectly matched layer for the absorption of electromagnetic waves. *J. Comput. Phys.*, 127:363–379, 1996.
22. L. Zhao and A.C. Cangellaris. A general approach for developing unsplit-field time-domain implementations of perfectly matched layers for FDTD grid truncation. *IEEE Trans. Microwave Theory Tech.*, 44:2555–2563, 1996.
23. F. L. Teixeira and W. C. Chew. Analytical derivation of a conformal perfectly matched absorber for electromagnetic waves. *Micro. Opt. Tech. Lett.*, 17:231–236, 1998.
24. P. G. Petropoulos. Reflectionless sponge layers as absorbing boundary condition for the numerical solution of maxwell's equation in rectangular, cylindrical, and spherical coordinates. *SIAM J. Appl. Math.*, 60(3):1037–1058, 2000.
25. E. Bécache, S. Fauqueux, and P. Joly. Stability of perfectly matched layers, group velocities and anisotropic waves. *J. Comput. Physics*, 188:399–433, 2003.
26. F. Hastings, J.B. Schneider, and S. L. Broschat. Application of the perfectly matched layer (PML) absorbing boundary condition to elastic wave propagation. *J. Acoust. Soc. Am.*, 100(5):3061–3069, November 1996.
27. F. Collino and C. Tsogka. Application of the PML absorbing layer model to the linear elastodynamic problem in anisotropic heterogeneous media. *Geophysics*, 66:294–305, 2001.
28. E. Bécache, P. Joly, and C. Tsogka. An analysis of new mixed finite elements for the approximation of wave propagation problems. *SIAM J. Numer. Anal.*, 37:1053–1084, 2000.
29. J.C. Nédélec. A new family of mixed finite elements in  $\mathbb{R}^3$ . *Numer. Math.*, 50:57–81, 1986.
30. E. Bécache, J. Rodriguez, and C. Tsogka. On the convergence of the fictitious domain method for the anisotropic wave equation. *preprint*, 2004.
31. E. Kjartansson. Constant Q wave propagation and attenuation. *J. Geophys. Res.*, 84:4737–4748, 1979.
32. G. Szego. Orthogonal polynomials. *Am. Math. Soc.*, 1939.
33. C. Brezinski. *Padé-type approximation and general orthogonal polynomials*. Birkhauser, 1980.
34. I. Babuska. The Finite Element Method with Lagrangian Multipliers. *Numer. Math.*, 20:179–192, 1973.
35. A. Wirgin, editor. *Wavefield Inversion*. Springer Verlag, 1999.
36. M.I. Todorovska, A. Hayir, and M.D. Trifunac. Antiplane response of a dike on flexible embedded foundation to incident SH-waves. *Soil Dynam. and Earth. Eng.*, 21:593–601, 2001.